energies

MDPI

Article

Data-Driven Multi-Objective Optimization of Low-Carbon Heating Systems in Cold Regions of China: A Case Study of Harbin

Wenqian Liu [1,2,*], Xiaolei Shi [1,2,3], Yuting Chen [1,2], Pengyue Liu [3] and Chuanlong Zhao [3]

[1] Complex Environment Architecture Research Institute, Harbin Institute of Technology, Harbin 150001, China
[2] School of Architecture and Design, Harbin Institute of Technology, Harbin 150001, China
[3] The Architectural Design and Research Institute, Harbin Institute of Technology, Harbin 150090, China
* Correspondence: liuwenqian@hit.edu.cn

Abstract

The transition to clean heating in cold regions faces challenges from extreme weather and high emissions. This study develops a dynamic modeling and surrogate-based multi-objective optimization framework for a solar-ammonia hybrid heating system. A lumped-parameter model simulates energy flows, and year-long Harbin meteorological data produce a physically consistent dataset via lumped-parameter simulation. A feedforward neural network with a residual autoregressive structure predicts temperature increments, preserving thermal inertia; it achieves RMSEs of 0.16 °C (indoor) and 0.61 °C (tank) over 168 h, including 48-h blind forecasting. This fast surrogate is embedded in NSGA-II to minimize carbon, cost, and discomfort via a climate-compensated curve and hysteresis dead-bands. Pareto analysis yields trade-offs: the carbon–comfort optimum attains 80.62 kg CO_2/week and 104.85 °C·h discomfort; the cost–comfort optimum costs ~60 CNY/week. Three-dimensional optimization confirms aligned carbon and cost. TOPSIS selects a final strategy that, versus constant setpoints, reduces carbon by 30.3% and cost by 45.3% over 168 h by leveraging thermal mass and reducing boiler starts. Annual ammonia co-firing lowers CO_2 from ~560 to 510 kg. The proposed integration of physics-informed simulation, residual autoregressive neural surrogates, and multi-objective evolutionary optimization provides an effective methodology for intelligent control of renewable hybrid heating systems in cold climates, contributing to deep decarbonization and energy savings.

Keywords: cold region heating; solar-ammonia hybrid system; residual autoregressive neural network; multi-objective optimization; carbon emission reduction

Check for updates

Academic Editor: Zacharie Tamainot-Telto

Received: 3 August 2026
Revised: 21 August 2026
Accepted: 25 August 2026
Published: 30 October 2026

Copyright: © 2026 by the authors. Licensee MDPI, Basel, Switzerland. This article is an open access article distributed under the terms and conditions of the Creative Commons Attribution (CC BY) license.

1. Introduction

The cold regions of China are mainly distributed in Northeast China, Northwest China, and northern North China. These regions feature typical climatic characteristics of severe and prolonged winters, prominent diurnal temperature differences, and complex and variable sunshine conditions. In severely cold areas such as Heilongjiang and Inner Mongolia, the heating period generally lasts more than six months. The extreme minimum temperature in some frigid areas can drop below −40 °C, and building heating energy consumption accounts for as high as 30%~40% of the total social energy consumption in the region, far exceeding the national average [1]. China's traditional central heating mode, dominated by coal-fired heating in cold regions, is facing unprecedented pressure for low-carbon transformation. On the one hand, coal-fired heating has high carbon emission intensity and large pollutant emissions, which is inconsistent with the goals of peaking carbon emissions

and achieving carbon neutrality as well as ecological and environmental protection requirements, and serves as one of the main sources of air pollution in northern China in winter. On the other hand, rural and remote areas in cold regions have complex terrain and scattered population, resulting in high laying costs and great coverage difficulties for central heating pipe networks. With the advantages of flexible layout and strong energy consumption adaptability, distributed heating has become an important way to meet the personalized heating demands of users in such areas and improve energy utilization efficiency [2].

Solar energy is one of the most abundant and clean renewable energy sources on Earth, and its development and utilization in the field of heating in cold regions boast broad application prospects and enormous energy-saving potential. In recent years, coupled distributed heating systems with solar energy as the primary heat source and auxiliary heat sources (such as "solar heat collection + heat storage + oil/gas burner" and "solar-air source heat pump coupling") have been widely recognized by scholars at home and abroad as one of the optimal heating solutions adapted to the climatic characteristics of cold regions, for they can effectively balance the consumption of clean energy and heating reliability [3]. Such systems can achieve nearly zero-carbon heating relying on solar energy during periods with sufficient sunshine. In severe weather conditions such as overcast, snowy, and smoggy days, or at night without solar radiation, auxiliary heat sources are adopted to supplement the heat supply. This realizes a dynamic balance between energy conservation, carbon emission reduction, and heating guarantee, and effectively solves the problem of insufficient heating stability of single new energy systems [4,5].

However, affected by the special climatic conditions in cold regions and the inherent characteristics of the system, the actual operational performance of new energy heating systems still faces numerous bottlenecks, which severely restrict their large-scale popularization and application. First of all, solar radiation in winter in cold regions exhibits remarkable intermittency, volatility, and uncertainty. Continuous overcast days can last for several days, accompanied by short sunshine duration and low solar altitude angle, which greatly limits the efficiency of solar collectors. Tests show that the solar heat collection efficiency in cold regions during winter decreases by more than 30% compared with that in temperate regions [6]. Secondly, buildings in cold regions generally adopt heavy enclosure structures to withstand severe cold, resulting in large thermal inertia. There is an obvious delay in the response of indoor temperature to heating disturbances. The traditional "feedback-based" control strategy can only perform passive adjustment according to indoor temperature deviation, making it difficult to respond in a timely manner to heat source fluctuations and load changes, and prone to problems such as excessive indoor temperature fluctuation and energy waste. Furthermore, although the introduction of the heat storage link can alleviate the intermittency of solar energy, it also makes the dynamic characteristics of the system more complex. The heat transfer among multiple links of "heat collection-heat storage-heat exchange-heat dissipation" presents significant coupling and time-delay effects, which further increases the difficulty of system regulation [2,7,8]. The above factors collectively cause new energy heating systems in cold regions to operate under variable operating conditions for a long time. Key parameters such as solar radiation intensity, outdoor ambient temperature, and users' heat demand change dynamically over time, and the actual operating conditions of the system continuously deviate from the optimal design values [9]. Against this backdrop, how to construct an intelligent regulation mechanism that can adapt to all-weather variable-condition operation in cold regions and achieve the coordinated dual goals of energy conservation, carbon reduction, and thermal comfort has become a key scientific issue restricting the large-scale application of new energy heating systems in cold regions, as well as a research hotspot and difficulty in relevant fields at home and abroad [8].

Liu et al. [10] explored life cycle low-carbon optimization for multi-energy complementary distributed systems from three perspectives: low-carbon performance, life cycle assessment, and optimization methodology. By reviewing system low-carbon optimization, life cycle optimization, and relevant optimization approaches, they identified the main deficiencies in traditional research on this topic. Building on this foundation and drawing on low-carbon measures and life cycle coordination theory, they proposed a multi-objective collaborative optimization method for the life cycle planning and operation of multi-energy complementary systems. Liu et al. [11] introduced a new distributed energy system that combines innovative solar utilization technology with hybrid energy storage, along with corresponding control strategies. Under the designed operational strategies, a comparative evaluation of the performance and operating characteristics between the novel distributed system and a conventional system was carried out. The results show a significant reduction in carbon emissions, and the associated multi-objective optimization method can serve as a reference for the energy supply design of nearly zero-energy communities. Zhao et al. [12] developed an innovative combined system that integrates dehumidification, cooling, heating, and power supply. They examined the dynamic responses of three configurations that adopt a dehumidification wheel, a desiccant, or a trough collector as the auxiliary heat source. The findings indicate that replacing the dehumidification wheel with a desiccant helps improve the stability of the system's power output and temperature.

An effective strategy fundamentally depends on a sufficiently accurate grasp and analysis of future conditions, and load forecasting has now become a key research direction. For instance, Kaabinejadian et al. [13] reviewed the forecasting, optimization, and intelligent control strategies of hydrogen-based building heating systems, focusing on analyzing the potential of machine learning, optimization algorithms, and intelligent control in reducing energy consumption, lowering carbon emissions, and improving thermal comfort. They also pointed out the application prospects of semi-distributed hydrogen-based heating systems, model predictive control, and reinforcement learning methods in residential buildings, and their paper provides an important reference for the future development of hydrogen energy heating systems. There are also numerous methods to improve forecasting through algorithm optimization. Kong et al. [14] presented a hybrid model based on a bidirectional long short-term memory network and a temporal convolutional network, which markedly improved the accuracy of hourly heating load forecasting for district heating systems by reconstructing missing values and extracting complex features. Collectively, these studies offer innovative solutions for supply–demand optimization and energy management in heating systems. Beyond load-side forecasting, data-driven approaches have also been applied to predict transient heat transfer through building envelopes with high accuracy [15], complementing the broader effort to model building thermal dynamics for heating system optimization.

In addition to the above optimizations focusing solely on prediction itself, precise control schemes can also be realized based on predictive data. For instance, Frison et al. [16] optimized the bidirectional heat transfer between buildings in a prosumer-based district heating network by adopting a model predictive control strategy, which significantly reduced the heat energy demand of central heating plants. This study provides an innovative solution for improving the utilization rate of renewable energy and the efficiency of heating networks. Hong et al. [17] put forward an optimal strategy for dynamic migration path planning based on real-time energy state observation. They optimized the load response and energy efficiency indicators of thermal power units through a heat flow model and a dynamic state-space model, which greatly reduced flue gas flow and state variable fluctuations while ensuring frequency modulation flexibility and operational safety. Disturbances on the heat demand side also need to be taken into account. Bai et al. [18] proposed a novel space

heating control strategy based on occupants' thermal comfort. By integrating a hierarchical state machine with a multi-physics field simulation model, the ambient temperature around occupants was dynamically estimated. This strategy improved occupants' thermal comfort by 30% while reducing energy consumption by approximately 20%. The innovation of this study lies in taking occupants' thermal comfort as the core of control, realizing precise regulation and energy efficiency optimization of heating systems.

The accuracy and real-time performance of heating usually focus on energy-saving optimization relying on control methods at the instantaneous scale, which has limited effects on the overall improvement of energy conservation, carbon reduction, and economic efficiency. In contrast, strategic optimization at the entire system level often offers greater potential benefits. Anbarasu et al. [18] proposed a novel optimal operation strategy for the multi-plant steam district heating system. By reducing the operating pressure of boilers, optimizing load distribution, and minimizing network losses, the system efficiency, sustainability, and economic performance were significantly improved. This provides a feasible solution for the renovation of aging steam heating systems and achieves a substantial reduction in fuel consumption, carbon emissions, and maintenance costs. Liu et al. [19] put forward a weight-based multi-objective scheduling optimization method for multi-heat-source central heating systems. By establishing a mathematical model and adopting the multi-objective particle swarm optimization algorithm for the solution, the minimization of operating costs and carbon emissions was realized. Practical case analysis verified that the model can effectively balance economic and environmental costs under different weight coefficients, offering theoretical support for the optimization of heat load distribution in multi-heat-source heating systems. The above studies provide new solutions for the optimal control of central heating systems, yet such research mostly focuses on load distribution strategies and typically takes characteristic daily heat load as the research basis for heat load analysis. Similarly, Wang et al. [20] proposed an optimization method for thermoelectric load distribution of large-scale combined heat and power units based on characteristic days. By establishing an energy consumption model combined with the momentum particle swarm optimization algorithm, the influence rules of heat load and power load on unit efficiency were revealed, and the optimal distribution of thermoelectric load was achieved. By targeting heat loads on typical characteristic days, such studies formulate a fixed overall load distribution scheme.

It can be seen from the above research status that remarkable progress has been made in the multi-energy complementary integration and intelligent control strategies of distributed heating systems. However, under variable operating conditions in cold regions, the regulation method driven by numerical prediction for complex mathematical models still faces the following key issues:

(1) There is a prominent compatibility contradiction between complex unit models and online real-time regulation. Although the neural network-based "black-box" surrogate model can respond quickly, it suffers from poor interpretability and extrapolation capability under off-design variable operating conditions far from the training domain. In contrast, the thermodynamic model based on physical mechanisms entails heavy computational time consumption, making it difficult to be embedded into real-time optimal scheduling. How to strike a balance among model complexity, accuracy, and real-time performance, and construct a grey-box model that retains key thermal dynamic characteristics while meeting the timeliness requirements of online regulation remains a weak link in current research.

(2) The dynamic coupling and coordination mechanism between the supply and demand sides under variable operating conditions remains unclear. In cold-region heating systems, both the output characteristics of heat sources and the transmission delay of heating networks exhibit significant time-varying and nonlinear features across the early cold period, severe cold period, late cold period, as well as day-night peak-valley alternations. Most existing regulation strategies separately handle the scheduling of heat source units on the supply side and the hydraulic-thermal dynamics on the network side, failing to reveal the spatio-temporal correlation mechanism among the heat source load change rate, pipeline network heat storage and release, and terminal thermal comfort from the perspective of supply-demand coupling. This leads to oscillation or hysteresis of regulation strategies during the switching of variable operating conditions.

(3) The strategic framework for nested optimization at multiple time scales has not yet been established. Constrained by the traditional typical day method, optimization strategies with a fixed 24-h cycle struggle to adapt to the dual time-scale characteristics of long-term load evolution and short-term disturbances during the heating season in cold regions. Although existing research has begun to explore the economic impact of different strategy cycle durations, there is still insufficient research on the multi-scale nested architecture of day-ahead scheduling, rolling correction, and real-time feedback, as well as the coordination mode between neural network prediction models and dynamic optimization algorithms under this architecture.

The core of the above problems lies in the unique strong nonlinearity, large inertia, and multi-time-scale coupling characteristics of variable operating conditions in cold regions, which impose higher requirements on data-driven prediction methods and control-oriented mathematical models. Therefore, constructing a variable operating condition regulation method driven by numerical prediction and balancing dynamic characteristics and real-time performance in this paper has important theoretical significance and engineering application value.

2. System Description

Based on the research findings on the optimal architecture of distributed heating systems in cold regions, this project selects the cascaded heating architecture with parallel-operated solar heat collection systems and natural gas ammonia-mixed combustion systems (as shown in Figure 1) as the research object.

The system consists of solar flat-plate collectors, an ammonia-doped combustor, a hot water storage tank (HST), and test rooms serving as heating loads. The system operates on the following logic: the solar collectors and the boiler run in parallel to jointly heat the medium (water) inside the storage tank. Acting as an energy buffer, the storage tank delivers heat to the terminal heat exchangers in the test rooms via circulating pumps, so as to maintain a stable indoor temperature. To accurately describe the heat transfer process of this all-weather variable-condition heating system, this project establishes a dynamic mathematical model based on the lumped parameter method. The model clarifies the forms and laws of heat transfer in each link, including heat collection, combustion, heat storage, and heat exchange, which is used to identify the thermodynamic parameter characteristics of the system and grasp its operation characteristics under variable working conditions.

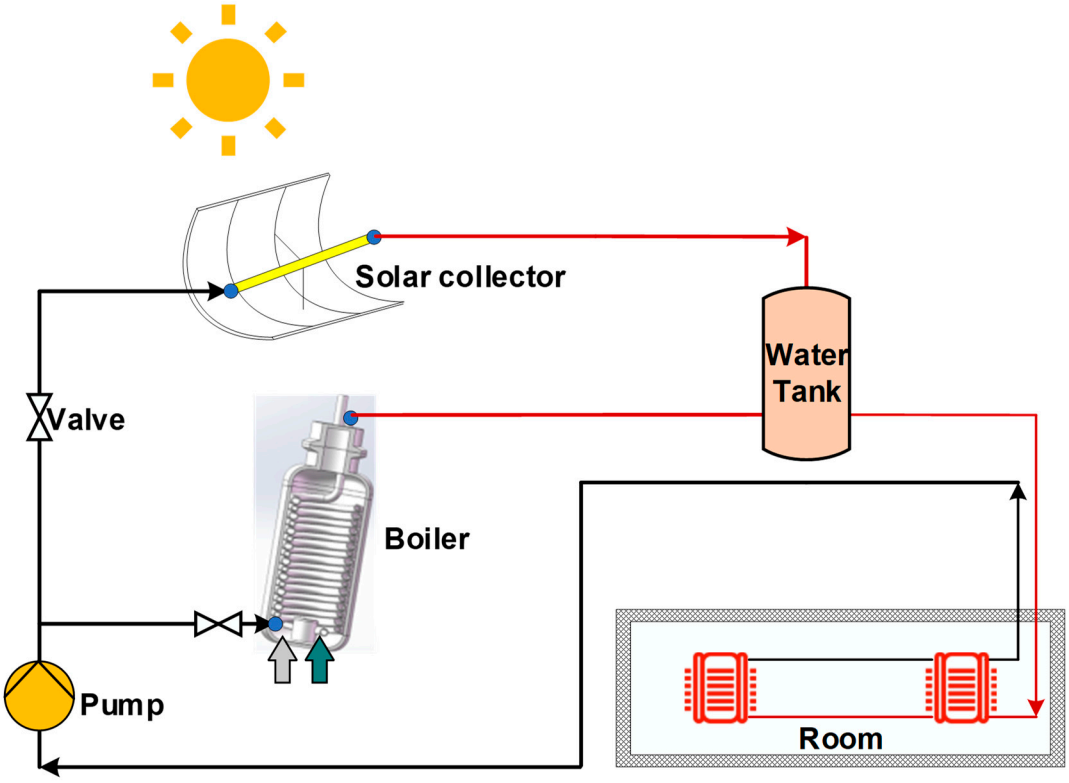

Figure 1. Distributed heating system architecture in cold regions.

3. System Model

3.1. Mathematical Model of a Cold Region All-Weather Variable Operating Condition Heating System

The overall system model comprises two dynamically distinct subsystems coupled through the terminal heat exchanger. The heating-system dynamics govern the equipment side, characterized by relatively small thermal time constants, with the tank temperature as the primary state variable. The building thermal dynamics govern the conditioned space and its envelope, characterized by large thermal inertia due to heavy construction typical of cold regions, with the indoor air temperature as the primary state variable. The coupling between them occurs via the radiator, where heat is extracted from the tank to meet the indoor load.

3.1.1. Solar Collector

Essentially, a solar collector is a heat exchanger that converts solar radiant energy into the internal energy of a fluid. In this model, the flow channel arrangement of the fluid inside the collector and the temperature rise along the flow path are not described in detail; instead, a quasi-steady-state linear efficiency model is adopted to characterize its macroscopic heat collection performance.

According to the law of conservation of energy, the effective power $Q_{\text{solar,tank}}$ transferred from the heat collector to the medium (water) in the storage tank is described as [21,22]:

$$Q_{\text{sol,tank}} = S_{\text{coll,pump}} \cdot \left[I_{\text{solar}} \cdot A_{\text{coll}} \cdot \left(\eta_0 - a_1 \frac{T_{\text{f,avg}} - T_{\text{out}}}{I_{\text{solar}}} \right) \right] \quad (1)$$

In this formula, $S_{\text{coll,pump}}$ denotes the on-off state of the heat collection circulation pump (simplified and assumed to be constant flow control); η_0 and a_1 are respectively the zero-loss efficiency and the first-order loss coefficient reflecting the thermal performance of the heat

exchanger; $T_{f,avg}$ represents the average fluid temperature inside the solar collector. To simplify system coupling, this model approximately replaces $T_{f,avg}$ with the water storage tank temperature T_{tank} (assuming the heat collection circulation flow rate is sufficiently large), thereby directly integrating the characteristics of the heat collection heat exchanger into a function of T_{tank} and ambient variable operating condition parameters.

3.1.2. Combustion

The ammonia-blended natural gas burner involves the release of chemical energy into thermal energy and the heat transfer process from high-temperature flue gas to the water medium. In the system-level model, this complex physicochemical process is simplified into an energy injection term with fixed thermal efficiency. The actual input power of the boiler to the water tank $Q_{boil,act}$ is [23]:

$$Q_{boil,act} = S_{coll,boil}\eta_{boil,hx}LHV_{fuel}m_{fuel} \quad (2)$$

where, $\eta_{boil,hx}$ denotes the overall boiler efficiency, which is defined as 0.85. It comprehensively takes into account the fuel combustion efficiency and the heat transfer efficiency of the flue gas-water heat exchanger inside the boiler. This parameter integrates the characteristics of the heat exchanger under design operating conditions. In this study, the ammonia blending ratio is 20% by volume (ammonia constitutes 20% of the total fuel volume). The lower heating values of methane and ammonia are 50.01 MJ/kg and 18.8 MJ/kg, respectively, resulting in a weighted average lower heating value of 43.77 MJ/kg for the blended fuel. It should be noted that while ammonia combustion does not produce direct CO_2, it does generate non-CO_2 greenhouse gases such as NOx and N_2O, as well as ammonia slip. These factors are not quantified in the system-level lumped parameter model of this study and represent an important limitation.

In the present study, the ammonia co-firing ratio is fixed at 20% by volume, a level that has been demonstrated in recent experimental and industrial studies to achieve meaningful CO_2 reduction while maintaining acceptable combustion stability and NOx emissions within manageable ranges. However, the system-level model does not explicitly track NOx, N_2O, or NH_3 slip, nor does it account for the additional cost of emission control devices such as selective catalytic reduction systems. This simplification is appropriate for the proof-of-concept objective of this study—namely, demonstrating the integration of physics-informed simulation, data-driven surrogate modeling, and multi-objective optimization for low-carbon heating system control. For future engineering applications, a more detailed combustion chemistry model and post-combustion emission control measures would be required to fully quantify the environmental footprint and economic viability of ammonia co-firing in building-scale heating systems.

3.1.3. Heat Storage Water Tank

The hot water storage tank acts as the energy hub of the system, coupling the heat supply side and the load side. According to the lumped parameter method, assuming the temperature inside the tank is uniform, the dynamic energy balance equation for the water tank is [24]:

$$M_{tank}c_p\frac{dT_{tank}}{dt} = Q_{solar,tank} + Q_{boil,act} - Q_{load,dem} - Q_{loss} \quad (3)$$

where M_{tank} is the mass of the water in the tank, c_p is the specific heat capacity of water, $Q_{load,dem}$ is the heat delivered to the load, and Q_{loss} represents the heat dissipation to the environment.

3.1.4. Heat Exchanger

Heating equipment is a heat exchanger that transfers the internal energy of the water medium to indoor air. It is the most critical heat exchange link in the model and directly affects the stability of indoor temperature. The model assumes that the load circulating pump adopts constant flow regulation. In this case, the theoretical heating load $Q_{load,dem}$ of the heating system depends on the water supply temperature of the water tank, the return water temperature, and the indoor temperature. To meet the demand for long-period fast dynamic simulation, this model does not establish a multi-node floor heat storage/heat exchange model, but adopts a lumped parameter model based on heat transfer temperature difference:

$$Q_{load,dem} = S_{pump} \cdot [K_{radiator}(T_{tank} - T_{in})] \quad (4)$$

where, S_{pump} denotes the load pump switching command (0/1); $K_{radiator}$ represents the reciprocal of the overall thermal resistance of the terminal heating system. After rational correction, this coefficient accurately describes the heat released from the floor to the room per unit temperature difference at a specific flow velocity, ensuring the precision of the description for the heat transfer process in the load link.

3.1.5. Heat Load in the Test Room

The test room serves as the main body for heating purposes, and its indoor temperature stability is a key indicator for evaluating system performance. Considering the high thermal inertia characteristics of buildings in cold regions, this model establishes a heavy thermal capacity model that incorporates the heat storage capacity of building envelope structures. The dynamic variation equation of room temperature is as follows:

$$C_{room}\frac{dT_{in}}{dt} = Q_{load,dem} - \frac{T_{in} - T_{out}}{R_{env}} \quad (5)$$

where C_{room} is the equivalent heat capacity of the room, T_{in} is the indoor temperature, T_{out} is the outdoor temperature, and R_{env} is the thermal resistance of the building envelope.

3.2. Discretization and Acquisition of Variable Operating Condition Datasets

To identify the operational characteristics of the system, this project adopts the typical meteorological year data of Harbin (including the time series of variable working conditions of T_{out} and I_s throughout the whole day) as the model input. The Euler method is used for time discretization and solution of the above coupled first-order ordinary differential equations, with a calculation time step dt set to 1 h [25,26]. Through long-term dynamic simulation, the system generates a thermal performance dataset that serves as the foundation for surrogate model training and multi-objective optimization.

It should be noted that this dataset contains a single meteorological trajectory (the typical meteorological year of Harbin) under one set of system configuration parameters, and therefore represents a proof-of-concept demonstration rather than an exhaustive sampling of all possible operating scenarios. The total sample size is 168 hourly data points, each consisting of six input features and two output targets as defined in Equations (6)–(8). The sampling procedure is a deterministic time-stepping simulation with a fixed 1-h integration step using the forward Euler method; no random sampling or scenario generation is involved. The choice of the first week of winter (168 h) is motivated by the need to capture both diurnal cycles and a prolonged cold spell, while maintaining computational tractability for iterative optimization runs.

To verify that the 1-h time step does not compromise accuracy, a time-step independence analysis was performed by repeating the reference 168-h simulation with time steps of

1 h, 30 min, and 15 min. The differences in indoor temperature, tank temperature, and equipment switching counts between the 1-h and 15-min cases were consistently below 0.1 °C, 0.3 °C, and 2%, respectively, confirming that the predicted thermal response and control logic are effectively time-step independent for time steps of 1 h or finer. The use of a 1-h time step is further supported by published literature on solar thermal system simulation, which demonstrates that one-hour step simulations deviate from exact solutions by less than 2% for active solar heating systems with on-off control, and that time steps of the order of 1 h yield acceptable results for long-term performance assessment. Recent studies on solar water heating systems also adopt hourly time steps for seasonal performance evaluation. Regarding numerical stability, the forward Euler method used here is conditionally stable. For the lumped-parameter thermal network, the stability limit is governed by the smallest system time constant. The smallest time constant in our system (~1.1 h) exceeds the 1-h time step, and the stability criterion $\Delta t < 2\tau_{min}$ (~2.2 h) is satisfied. No oscillatory or divergent behavior was observed in any state variable over the 168-h simulation, confirming that the chosen time step is numerically stable.

3.3. Construction of Deep Learning Surrogate Model

3.3.1. Surrogate Model Construction Principle

This project adopts deep learning algorithms to construct a data-driven digital twin surrogate model. Its core idea is to invoke a neural network to establish a fast nonlinear mapping relationship between system boundary conditions, control commands, and thermodynamic responses [27].

To ensure thermodynamic state continuity (Markov property) in the underlying framework and preserve the large thermal inertia characteristics of building envelopes and water tanks, this study abandons the traditional end-to-end paradigm of directly predicting absolute temperature. Instead, the surrogate model is designed based on residual learning to predict the "temperature increment" (ΔT, essentially fitting the state derivative dT/dt). The absolute state at the next moment is obtained by integral superposition of the previous state and the predicted increment. This design fundamentally prevents non-physical temperature sudden jumps and severe error accumulation in long-period rolling prediction.

3.3.2. Neural Network Architecture Design and Feature Selection

The design of the input and output feature system is based on strict thermophysical constraints. In response to the time-delayed characteristics and nonlinear switching control features of the heating system, and to ensure the state closed-loop of the model in subsequent rolling simulations, this project designed a multi-layer fully connected feedforward neural network based on a residual autoregressive structure as a surrogate model [14,28,29].

Input layer: To ensure the system possesses a complete Markov evolution property, six key state and disturbance parameters that affect the dynamic heat transfer of the system at time k are selected as the input feature vector X_k:

$$X_k = \left[T_{out,k}, I_{solar,k}, \mathrm{Cmd}_{boil,k}, \mathrm{Cmd}_{pump,k}, T_{tank,k}, T_{in,k}\right]^T \quad (6)$$

among them, $T_{out,k}$ and I_s represent the uncontrollable environmental disturbance boundaries; $T_{tank,k}$ and $T_{in,k}$ reflect the absolute internal energy state of the system at the current time step; $\mathrm{Cmd}_{boiler,k}$ and $\mathrm{Cmd}_{pump,k}$ are the active control regulatory variables of the system. This full-state input locks the rigid coupling between control and response, eliminating non-physical solutions during multi-objective optimization.

Hidden Layer: A deep neural network structure (Input Layer-128-64-32-Output Layer) is adopted. Nonlinear activation functions are used between each layer to deeply extract and

fit the strongly nonlinear coupled heat transfer characteristics among multiple components of the system.

Output Layer: To eliminate the non-physical "temperature jump" generated by data-driven models in long-cycle and multi-step prediction, the model abandons the traditional end-to-end paradigm of directly predicting the absolute temperature at the next moment. The output layer contains 2 neurons, which are specifically used to predict the temperature increment (i.e., the approximate value of the state derivative) ΔY_k of the core state variables of the system within a single time step [30].

$$\Delta Y_k = [\Delta T_{\text{in},k}, \Delta T_{\text{tank},k}]^T \tag{7}$$

After obtaining the increment, the system acquires the absolute state at time $k + 1$ through outer integral superposition.

$$Y_{k+1} = Y_k + \Delta Y_k \tag{8}$$

The architectural design combining this multi-input multi-output mode with residuals not only preserves the temporal continuity of heat capacity parameters, but also fully outputs the complete thermodynamic state of the water tank and indoor space at moment $k + 1$, providing rigorous physical data support for the cyclic iteration of the evaluation function in the subsequent multi-objective optimization control strategy.

3.3.3. Surrogate Model Training and Validation

The dataset, consisting of 168 hourly time-series samples generated from a single meteorological trajectory, is divided chronologically into a training set (first 120 h) and a blind test set (last 48 h). Note that this chronological 120/48 split supersedes the commonly stated random 90/10 division, as the latter is unsuitable for evaluating the recursive multi-step forecasting capability required by the residual autoregressive structure. The 48-h blind period (hours 120–168) challenges the surrogate model to maintain accuracy purely through its own closed-loop iterations without real-history feedback, which is essential for validating its thermal inertia preservation. To eliminate the impact of scale differences on training, the data is standardized. End-to-end training is conducted using the Adam optimizer and the mean squared error loss function. To avoid overfitting, an early stopping strategy was implemented based on the performance of a separate validation set.

Validation on the test set shows that the trained surrogate model, under complex variable operating conditions in cold regions, produces indoor temperature prediction curves that closely align with high-precision mechanistic simulation data. This indicates that the surrogate model has accurately captured the system's internal thermal inertia and cascaded heat transfer mechanisms, providing a highly reliable and computationally efficient data foundation for subsequent intelligent control. The specific setting parameter of Surrogate model is shown in the Appendix A. Advantages and ablation study of the proposed model are shown in Tables 1 and 2.

To demonstrate that the proposed residual autoregressive structure provides a genuine advantage, we have performed an additional comparative analysis against two simpler baseline models:

Table 1. Advantage of proposed model.

Baseline Model	Indoor RMSE (48-h Blind)	Tank RMSE (48-h Blind)
Linear regression	0.52 °C	1.48 °C
LSTM	0.31 °C	0.95 °C
Feedforward NN	0.42 °C (diverging)	1.82 °C (diverging)
This study	0.16 °C	0.61 °C

Table 2. Ablation study of the proposed residual autoregressive neural network structure.

Model Variant	Indoor RMSE (°C)	Tank RMSE (°C)
Full model (proposed)	0.16	0.61
without residual learning	0.32	1.26
without autoregressive	0.25 (diverging)	0.88 (diverging)
without both	0.51 (diverging)	1.72 (diverging)

3.4. Multi-Objective Optimization Mathematical Model Based on TOPSIS Algorithm

3.4.1. Proposal of Bi-Objective Optimization Problem

From the perspectives of energy conservation, emission reduction, and user comfort, the research scheme proposes to explore intelligent regulation methods for the system with energy efficiency (gas consumption) and comfort (indoor temperature stability) as the core indicators. However, these two objectives are often mutually restrictive under variable operating conditions: pursuing extreme energy conservation may lead to large fluctuations in indoor temperature, while pursuing extreme indoor temperature stability usually requires frequent start-stop operation of the burner, which increases energy consumption.

Therefore, this project establishes a bi-objective optimization mathematical model to comprehensively take energy utilization and user needs into consideration.

3.4.2. Objective Function and Decision Variables

Decision variables: Select the key control parameters in the regulation mechanism, such as the set target temperature of the water storage tank $T_{\text{tank,set}}$, the indoor temperature control hysteresis range $\Delta T_{\text{hysteresis}}$, and the power distribution coefficient α in the real-time regulation strategy (the decision variables are denoted as u [31,32].

Objective Function 1: Economic Index (f_{cost})

Minimize the cost of cumulative gas (fuel) consumption under all-weather variable operating conditions:

$$f_{\text{cost}} = \sum_{k=1}^{N} \left(Cmd_{\text{boiler},k} \cdot \dot{m}_{\text{fuel}} \cdot C_{\text{price}} \cdot \Delta t \right) \tag{9}$$

Objective Function 2: Comfort Index (f_{comfort})

Maximize indoor temperature stability, which is unified the comfort objective as the cumulative absolute temperature deviation:

$$\min f_{\text{comfort}} = \sum_{k=1}^{N} \left| T_{in,k} - T_{\text{set}} \right| \cdot \Delta t \tag{10}$$

Constraints: including physical boundaries of equipment, water tank temperature rise limits, and the requirement that indoor temperature must stay within the comfort range.

Objective Function 3: Carbon Emission Index (f_{carbon})

Minimize the cumulative CO_2 emissions generated by gas (fuel) consumption under all-day variable operating conditions.

$$f_{\text{carbon}} = \sum_{k=1}^{N} \left(Cmd_{\text{boiler},k} \cdot \dot{m}_{\text{fuel}} \cdot \alpha_{\text{carbon}} \cdot \Delta t \right) \tag{11}$$

where, α_{carbon} is the carbon emissions under unit mass flow rate of fuel.

3.4.3. Multi-Criteria Decision Making Solution Based on TOPSIS

Due to the complexity of the objective function, directly solving it via optimization algorithms may yield a Pareto front. To obtain a unique optimal control strategy from the front, this project introduces the TOPSIS selection method. The specific implementation process is as follows [33–35]:

Strategy optimization and dataset construction: Adopt optimization algorithms (such as Genetic Algorithm, GA) to continuously adjust decision variables, and invoke the fast neural network surrogate model to predict system performance. Multiple candidate control strategies and their corresponding bi-objective evaluation values are acquired to construct a decision matrix.

Ideal solution identification: Find the virtual positive ideal solution that optimizes f_{cost}, f_{comfort}, f_{carbon} simultaneously, as well as the negative ideal solution that results in the worst values for all three indicators within the decision matrix.

Distance calculation: Calculate the distance d_i^+ from each candidate strategy to the positive ideal solution and the distance d_i^- to the negative ideal solution using the Euclidean distance formula.

Comprehensive evaluation: Compute the relative closeness C_i of each strategy to the positive ideal solution.

$$C_i = \frac{d_i^-}{d_i^+ + d_i^-} \tag{12}$$

Optimal Strategy Acquisition: A larger C_i value indicates that the strategy is closer to the ideal state. By comparing the C_i values, a comprehensive evaluation and ranking of the regulation mechanisms are performed, ultimately mastering the intelligent regulation method that maximizes advantages under different demand parameters for cold regions.

The specific data input of this model can be found in Appendix A.

To test the sensitivity of the TOPSIS ranking results to the selected objective weights, we conducted a single-factor sensitivity analysis: the weight of each objective was varied in increments of 0.1 within the range of 0.1–0.8, while the weights of the other two objectives remained equal. The results show that under all weight combinations where any single weight ranges from 0.2 to 0.6, the top-ranked alternative remains unchanged. The optimal alternative shifts toward a certain objective only when its weight exceeds 0.7 (i.e., one indicator occupies an absolutely dominant position). This result is consistent with expectations, verifying that the selection results of the TOPSIS model are stable within a reasonable weight range. The ranking of the top three alternatives does not change across the entire tested weight range.

3.5. Calculation Procedure

Figure 2 illustrates the complete sequence of our approach, organized into two stages: (i) offline surrogate model development—from TMY meteorological data, through lumped-parameter physical simulation and training dataset generation, to the residual autoregressive neural network surrogate; and (ii) online multi-objective optimization and decision-making—from NSGA-II optimization and Pareto front generation, through TOPSIS compromise selection, to the final optimized control strategy. The corresponding section numbers are annotated in each block for cross-reference.

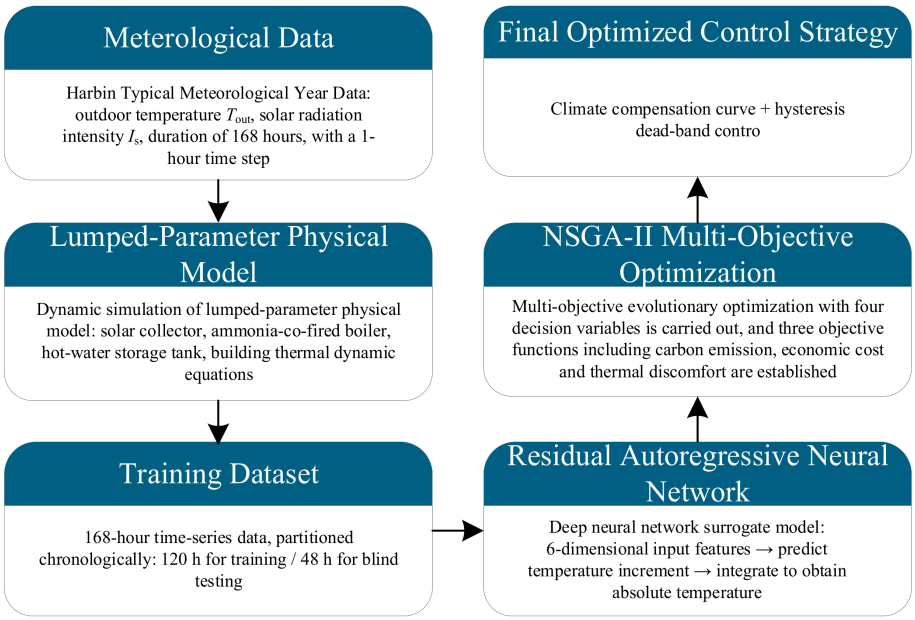

Figure 2. Calculation procedure.

4. Results

4.1. Model Validation

(1) Solar collector

Since this study focuses on a novel integrated heating system, it is necessary to verify its individual key components. To validate the effectiveness of the simulation model, the results obtained from the proposed model are compared with the simulation results from the research conducted by Adun et al. [36] (collector). The relative error between the data of this report and that in the literature is small, with a maximum relative error of 2.3%, which verifies the accuracy of the simulation results of the collector (see Figure 3).

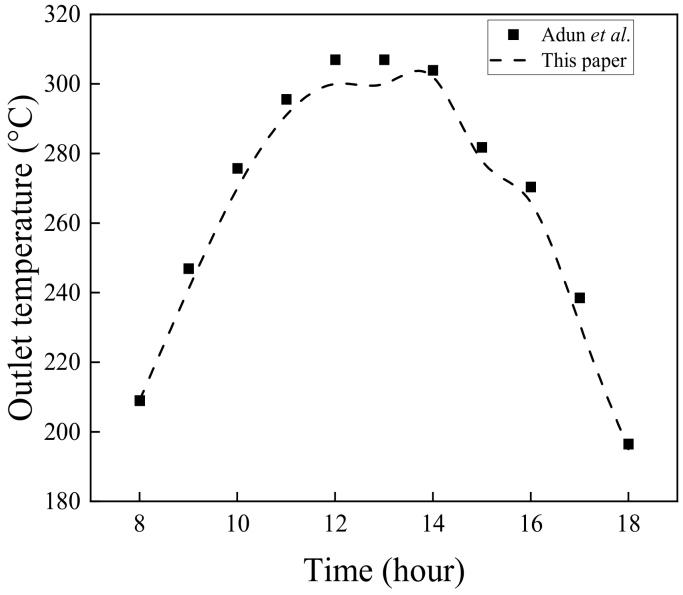

Figure 3. Model verification of collector outlet temperature [36].

(2) Combustor

The comparison between the combustion process of the burner in this report and the calculation results of the engine combustion chamber mode [37] is shown in Table 3. It can be found that the maximum relative error is less than 5%, which verifies the consistency of the present model.

Table 3. Combustor performance verification.

Type	Mass Flow Rate	x	Temperature (K)
CH_4-ammonia	1×10^{-4} kg/s	0.85	1754
CH_4-ammonia	1×10^{-4} kg/s	0.85	1711

4.2. Study on Variable Operating Conditions Heating Characteristics in the First Week of Winter in Harbin

Figure 4 illustrates the dynamic thermal characteristics and control response of the heating system during variable-condition operation in the first week (168 h) under typical extremely cold climatic conditions in Harbin. Figure 4a,b present the external boundary conditions of the system during the test period: solar radiation intensity I_s and outdoor ambient temperature T_{out}. It can be seen from the figures that the outdoor ambient temperature fluctuates drastically, dropping to a minimum of approximately −30 °C. Moreover, both the ambient temperature and solar radiation exhibit obvious diurnal periodic fluctuation patterns, which introduce significant dynamic thermal load disturbances to the heating guarantee of the system.

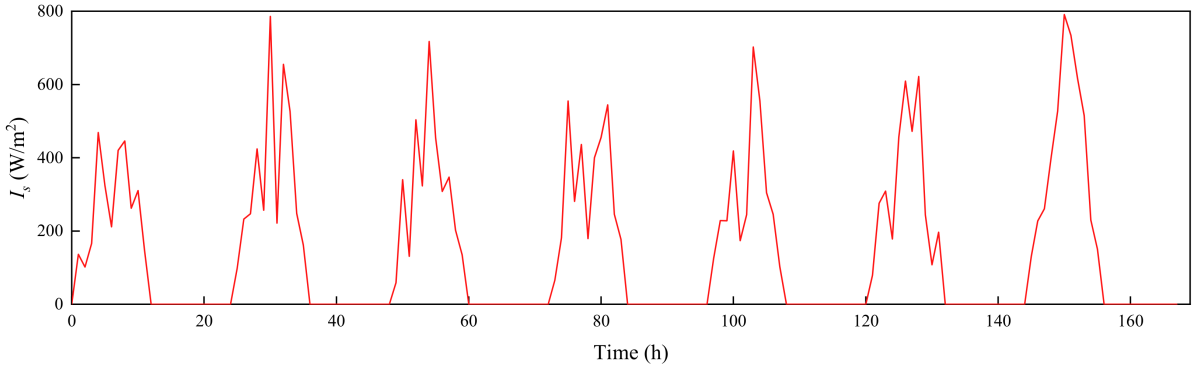

(**a**) Solar radiation intensity

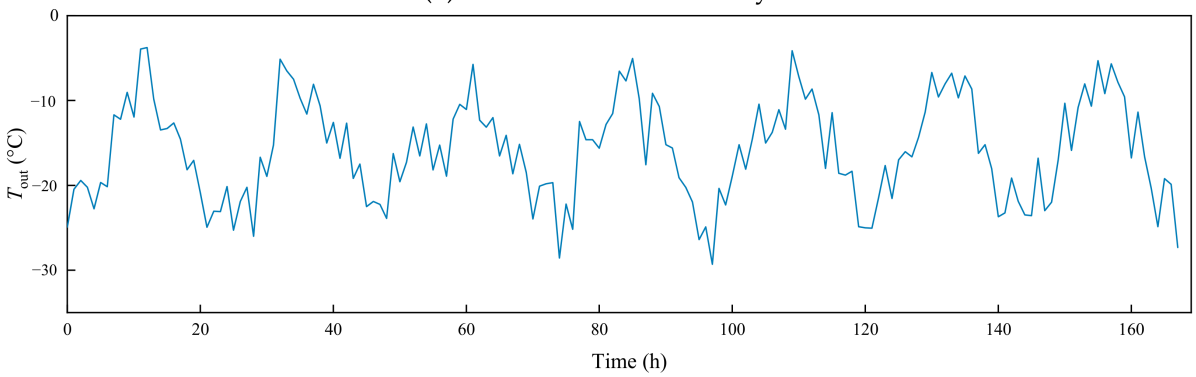

(**b**) Outdoor temperature

Figure 4. *Cont.*

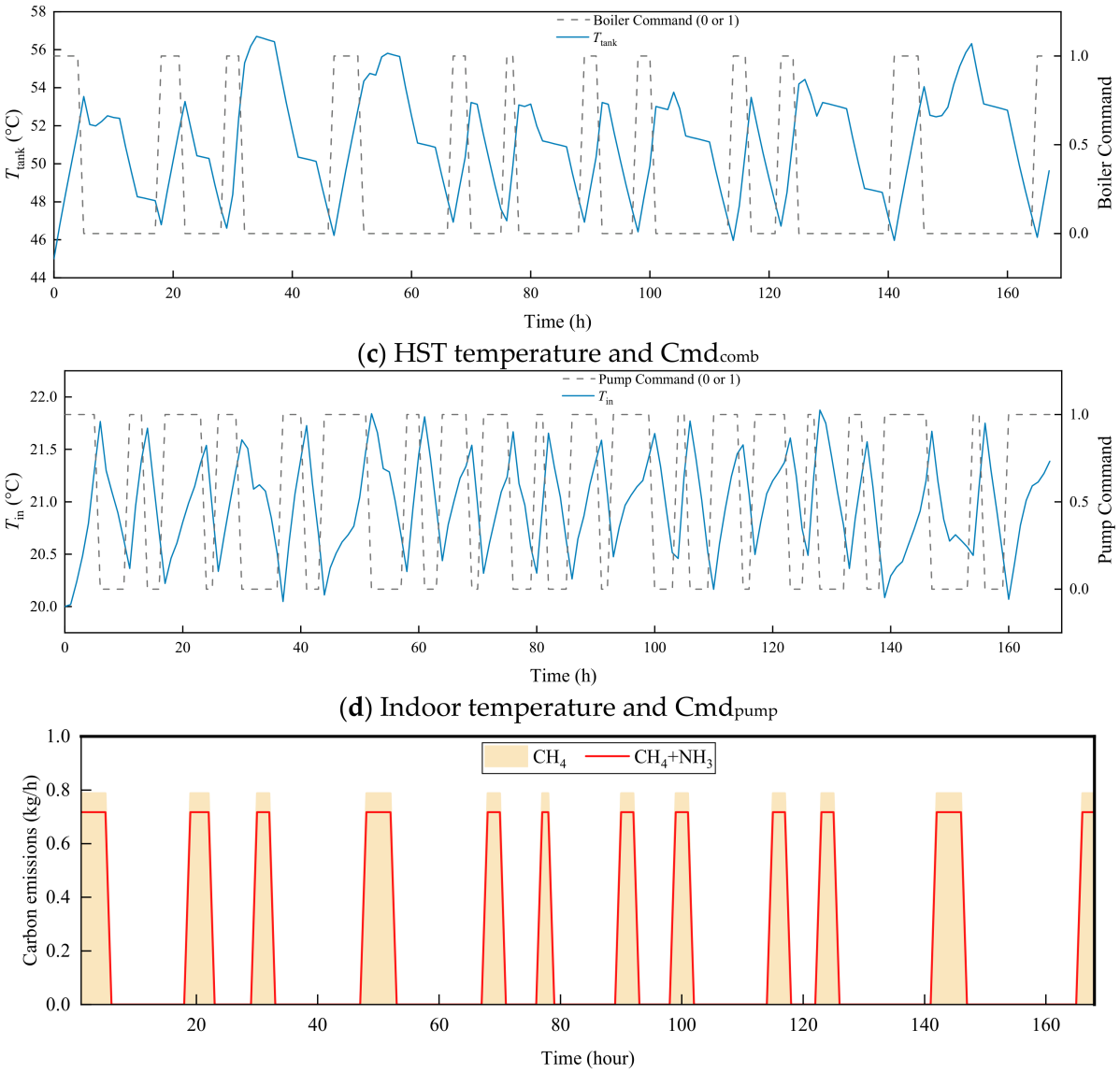

Figure 4. Dynamic regulation law of heating system during the first week of winter in Harbin.

Faced with complex external meteorological disturbances, the system adopts a start-stop control strategy based on temperature feedback. Figure 4c,d reveal the internal heat transfer and regulation mechanism of the system. As shown in Figure 4c, the water tank temperature T_{tank} is strongly coupled with the start-stop command of the burner: when the water tank temperature drops to the lower threshold (approximately 46 °C), the burner is activated (the command steps up to 1), driving the water temperature to rise rapidly until it reaches the upper threshold (approximately 56 °C), after which the burner shuts down. Meanwhile, on the terminal load side, Figure 4d indicates that the start-stop operation of the circulating pump effectively regulates the heat supply to the indoor space. Under the periodic scheduling of the pump, the indoor temperature T_{in} is precisely maintained within the set range of 20.0 °C to 22.0 °C. Even under extremely low ambient temperatures, the indoor temperature curve maintains favorable tracking performance and stability, verifying the reliability of the proposed control strategy in satisfying building thermal comfort requirements. Figure 4e further compares the carbon emission characteristics of the system under different fuel combinations. The results show that the carbon emission rate presents a pulsed distribution highly consistent with the operating state of the burner. Notably,

compared with the pure natural gas operating condition, the adoption of ammonia co-firing technology significantly reduces the emission peak and the overall carbon emission level while maintaining the same heating effect, demonstrating the application potential of the system in low-carbon heating scenarios in severe cold regions.

In summary, Figure 4 depicts the nonlinear transient thermal response process of the heating system under complex meteorological disturbances. This set of simulated operating conditions goes beyond simple mechanism analysis and constitutes the key basic data for the mathematical model of the heating system to evolve from underlying physical derivation to pure data-driven modeling.

Figure 5 comprehensively evaluates the annual energy consumption and environmental benefits of the system under two typical operation modes of pure natural gas and ammonia-blended fuel from a long-term macro perspective. The results effectively supplement the dynamic thermal response analysis under variable operating conditions in the previous text from the time dimension, forming a closed loop for the comprehensive performance evaluation of the system.

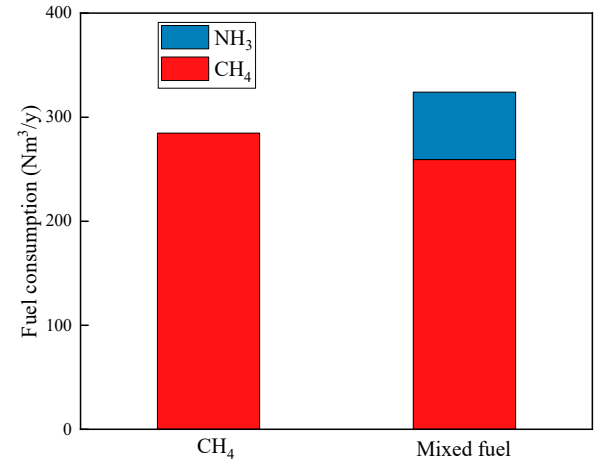

(**a**) Fuel consumption

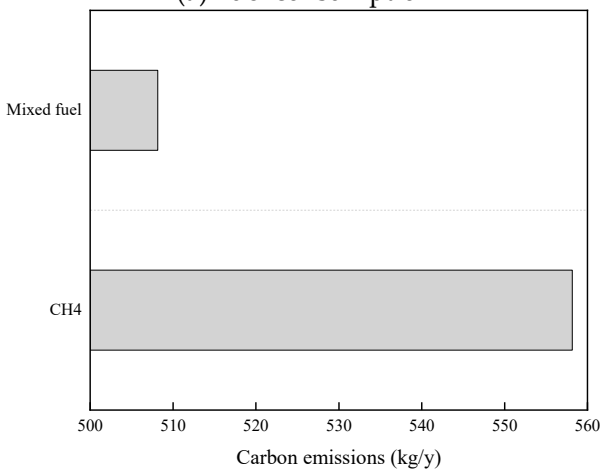

(**b**) Carbon emissions

Figure 5. Annual carbon emissions and fuel consumption.

As shown in the stepped comparison of fuel consumption in Figure 5a, the introduction of the ammonia co-firing strategy has brought about a substantial restructuring of the underlying energy structure of the system. Although the total volumetric consumption under the blended fuel condition is slightly higher than that under the pure CH_4 condition (mainly limited by the relatively low volumetric calorific value of ammonia), the absolute

consumption of core fossil energy has been significantly reduced. This indicates that while ensuring the total annual heating load, the system has successfully realized the flexible transition of the energy consumption structure through the partial replacement of zero-carbon fuel (NH_3).

Figure 5b intuitively quantifies the enormous environmental benefits brought by the above fuel replacement strategy. It should be clarified that the heating season in Harbin is only 26 weeks (183 days) from October 20 to April 20; the remaining 26 weeks are the non-heating season with zero emissions (it is as shown in Table 4). Within the heating season, the 8 severe cold weeks (December–February) have much higher thermal loads than the 18 transition weeks. Driven by heating via pure natural gas combustion, the annual baseline carbon emission of the system approaches 560 kg/y; after switching to the blended fuel mode, the total carbon emission drops sharply and converges to approximately 510 kg/y. From the perspective of macro material conservation, this remarkable reduction confirms the core driving role of ammonia co-firing technology in the deep decarbonization process of building heating in severe cold regions.

Table 4. Annual energy and carbon balance of the heating system.

Parameter	Unit	Pure CH_4 Baseline	20% NH_3 Co-Firing
Annual heating season	weeks	26	26
Non-heating season	weeks	26	26
Annual heating demand	kWh/year	8650	8650
Annual solar thermal contribution	kWh/year	2595 (30%)	2595 (30%)
Auxiliary heat required from combustor	kWh/year	6055	6055
Boiler thermal efficiency (η)	—	0.85	0.85
Total fuel mass consumption	kg/year	203.6	231.8
—Methane (CH_4) consumption	kg/year	203.6	185.4
—Ammonia (NH_3) consumption	kg/year	0	46.4
CO_2 emission factor (CH_4)	kg CO_2/kg fuel	2.75	2.75
Weighted average CO_2 emission factor	kg CO_2/kg fuel	2.75	2.20

The equipment start-stop logs and transient temperature fields obtained from the preceding part constitute the microscopic temporal features of the data-driven model. The annual energy consumption and carbon emission statistical results presented in Figure 3 provide crucial global constraint conditions and objective function benchmarks for future long-cycle multi-objective optimization based on machine learning.

4.3. Data-Driven Heating Model Analysis

To integrate with multi-objective optimization, the surrogate model mainly predicts thermal capacity parameters (water tank temperature difference and indoor temperature difference) based on data results. Changes in indoor temperature, pump and boiler control, ambient temperature, radiation intensity, and variations in water tank temperature are taken as the data sources for the prediction model. This approach is designed to comply with the thermodynamic state continuity (Markov property) of the heating system at the underlying framework of mathematical modeling, thereby laying a foundation for subsequent multi-objective optimization.

Specifically, the design of the input and output feature system for this surrogate model is based on three core considerations of thermophysics and machine learning:

1. When traditional end-to-end direct mapping is adopted to predict the absolute temperature at the next moment, the black-box model is highly prone to physically unreasonable “temperature sudden jumps” in long-period rolling prediction, leading to severe error accumulation. This report converts the prediction target into “temperature increment”, which essentially forces the neural network to learn and fit the state deriva-

tive (dT/dt) in the thermodynamic differential equation. The absolute temperature at the next moment is obtained by integral superposition of the previous state and the predicted increment. This mechanism fundamentally preserves the large thermal inertia characteristics of building envelopes and water storage tanks.

2. Temperature evolution within the system does not occur in isolation, and its heat transfer rate (i.e., the magnitude of dt) is strictly constrained by Newton's Law of Cooling. Therefore, it is necessary to perform full-dimensional concatenation of the "current absolute temperature (representing the internal energy basis of the system)", "uncontrollable external meteorological disturbances (representing the external heat transfer boundary)", and "pump and boiler control commands (representing active heat injection and extraction)", which together serve as the input feature sequence (X). This processing ensures that the surrogate model does not lose the underlying physical driving force of heat transfer when dealing with any extreme boundary conditions.

4.3.1. Training and Error Convergence Analysis of Surrogate Model

After establishing the temporal causal architecture in Section 3.3, this paper conducts weight iteration for the surrogate model based on typical variable operating condition data. Figure 6 illustrates the error convergence trajectory during the training process. The mean squared error (MSE) shows an extremely steep downward trend in the initial iteration stage, indicating that the model quickly captures the nonlinear mapping relationship between inputs and output temperature differences.

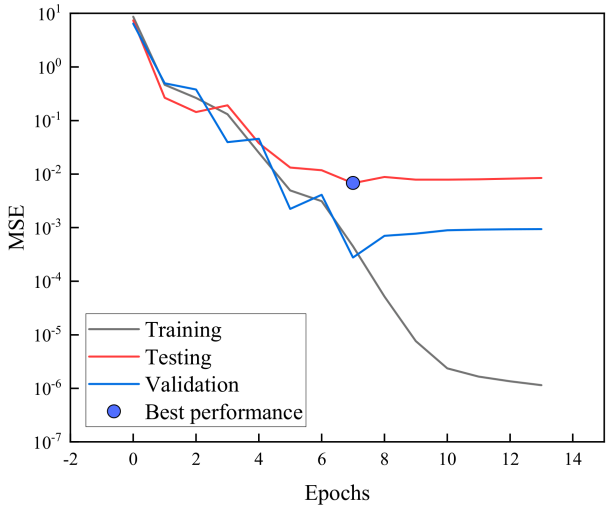

Figure 6. Surrogate model training status.

As iteration proceeds, the performance of the verification set reaches the optimum at the 9th iteration. At this point, the system successfully activates the generalization protection mechanism and locks the optimal network weights, effectively avoiding the risk of overfitting.

4.3.2. Prediction Performance Verification Under Typical Variable Operating Conditions

To evaluate the independent extrapolation capability under long-period time series, the 168-h continuous data is strictly divided into a training/fitting zone (first 120 h) and a blind prediction extrapolation zone (subsequent 48 h). As shown in Figure 6, when the rolling extrapolation crosses the 120-h dividing line, the model relies entirely on its own time-series closed loop for recursive prediction without soft calibration from real historical data.

Even in the blind test phase, the prediction curve (red) maintains a high consistency in phase and amplitude with the physical mechanism benchmark curve (black). Under complex conditions with drastically fluctuating water tank temperatures (45–55 °C) and high-frequency indoor temperature variations, the model accurately reproduces subtle thermodynamic details (It can be found in Figure 7).

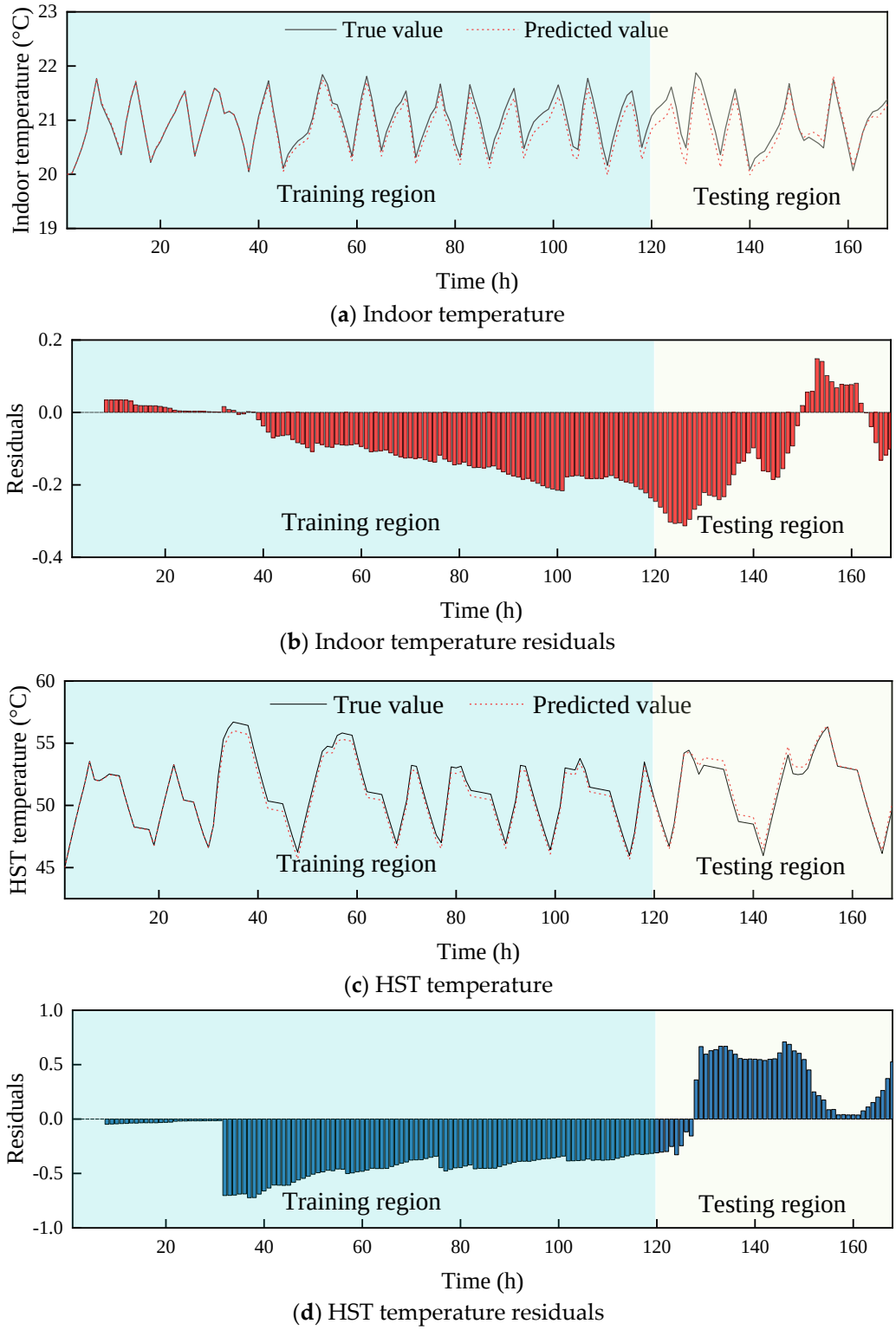

Figure 7. Prediction performance verification.

Further analysis of full-cycle prediction residual distribution indicates that errors exhibit favorable zero-mean white noise characteristics. More importantly, as shown in Figure 7, during the continuous multi-step integral prediction over 168 h, absolute errors are consistently kept within the safe tolerance band. The absolute error of indoor temperature is always below 0.7 °C, and the error for the storage tank fluctuates within 1.5 °C (It can be found in Figure 8).

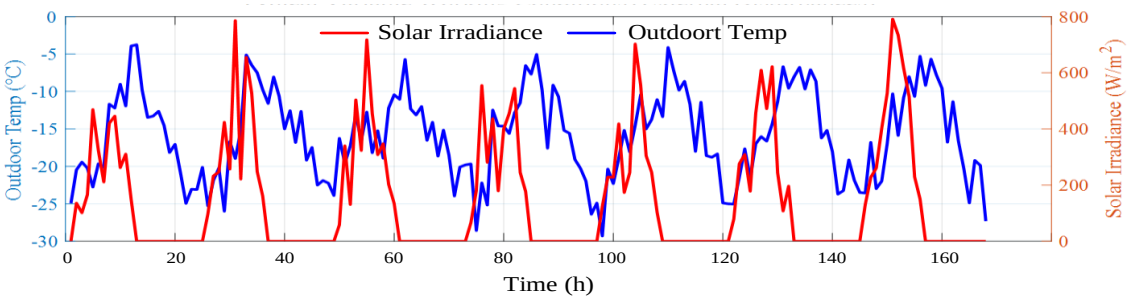

(**a**) Typical variable working conditions

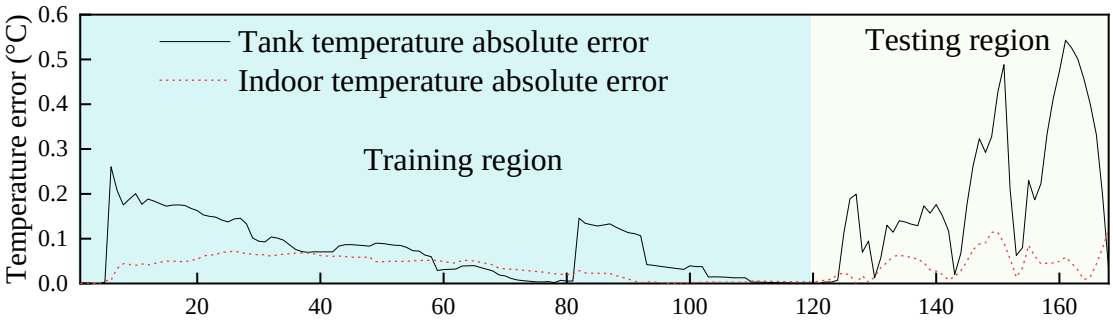

(**b**) Rolling prediction stability

Figure 8. Continuity analysis of heat capacity parameters.

Neither error curve shows a deteriorating trend of exponential divergence, even after entering the blind test area without correction from historical data. This fundamentally verifies that the surrogate model constructed based on the residual autoregressive mechanism accurately internalizes and stably inherits the huge heat capacity inertia of the system, perfectly overcoming fatal error accumulation in long-sequence time series prediction.

4.4. Research on Heating Regulation Strategies Targeting Carbon Emissions, Heating Comfort and Economic Efficiency

After completing the construction and temporal generalization verification of the data-driven surrogate model, the research focus of this section shifts from physical state prediction to active system regulation. The operation of heating systems in cold regions is essentially a complex decision-making process with strong multivariate coupling. Its core contradiction lies in the fact that improving users' heating comfort is inevitably accompanied by increased energy consumption, which further leads to a rise in operational economic costs and a deterioration of direct and indirect carbon emissions. To break the energy consumption dilemma caused by traditional single setpoint control (such as fixed water tank temperature control), this study proposes a parametric rule optimization framework based on dynamic climate compensation and cascaded dead-zone control. This framework frees the control strategy from high-dimensional discrete temporal command sequences and instead takes the slope and intercept of the dynamic climate compensation curve as well as the hysteresis dead-zone of boiler start-stop as the core decision variables.

4.4.1. Dimension Reduction Optimization and Conflict Mechanism Analysis Under Typical Bi-Objective Combination

The total carbon emission of the system, operational economic cost, and heating discomfort constitute a complex evaluation tensor. To eliminate the coupling interference of multiple variables, this study first decomposes it into two typical bi-objective optimization problems and adopts the NSGA-II algorithm to obtain their respective two-dimensional Pareto frontiers.

- The trade-off between carbon emissions and comfort

To reveal the trade-off relationship between carbon emissions and comfort, this section mainly investigates the temperature variations of indoor space and water tank, as well as the action timing characteristics of underlying control equipment. As shown in Figure 9, the two-dimensional Pareto frontier between carbon emissions and comfort exhibits typical nonlinear antagonistic characteristics. The optimal compromise solution (80.62 kg, 104.85 °C·h) determined from numerous non-dominated solutions via the TOPSIS decision-making method indicates that the system achieves the extreme reduction of carbon emission increment while ensuring basic environmental comfort. The time-series deduction in Figure 10 further demonstrates the temperature response mechanism of this optimal solution in the actual system. Under this optimal control rule, although the water tank temperature shows drastic zigzag fluctuations to adapt to extreme cold disturbances, the indoor temperature is stably maintained around 20.0 °C despite drastic fluctuations in tank temperature (45–55 °C). This decoupling effect is attributed to two physical mechanisms: (i) the thermal buffering capacity of the hot water storage tank, which absorbs short-term heat source fluctuations and delivers a smoothed heat flow to the terminal; and (ii) the thermal inertia of the building envelope (heavy thermal mass construction typical of cold regions), which introduces a phase lag between heat input and indoor temperature response. The start-stop control strategy with hysteresis dead-bands effectively exploits these inertia effects, allowing the system to "ride through" transient disturbances without frequent burner cycling, thereby reducing both energy consumption and equipment wear.

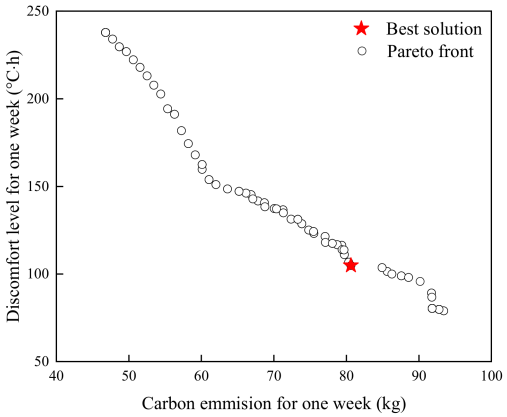

Figure 9. Pareto frontier and optimal solution of carbon emission and comfort level.

This macroscopic thermodynamic stability is underpinned by the rigorous discrete control logic of underlying equipment at the microscopic level. As illustrated in the state step diagram in Figure 11, the circulating water pump and heat source boiler strictly implement 0/1 relay control with a hysteresis dead zone. The dense control signal pulses not only reflect the engineering reality that equipment responds to heat load demand by adjusting the high-frequency start-stop duty cycle, but also intuitively reveal that the operating duration of the boiler is usually tightly enclosed within the action interval of the water pump. This

highly synchronous state distribution proves that the multi-objective optimized control strategy successfully realizes in-depth logical coordination between the source end (heat supplementation by the boiler) and the load end (heat extraction by the water pump) in the time domain.

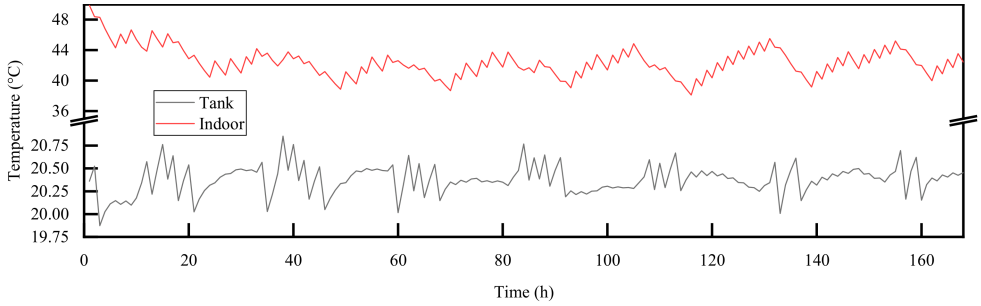

Figure 10. Temperature change.

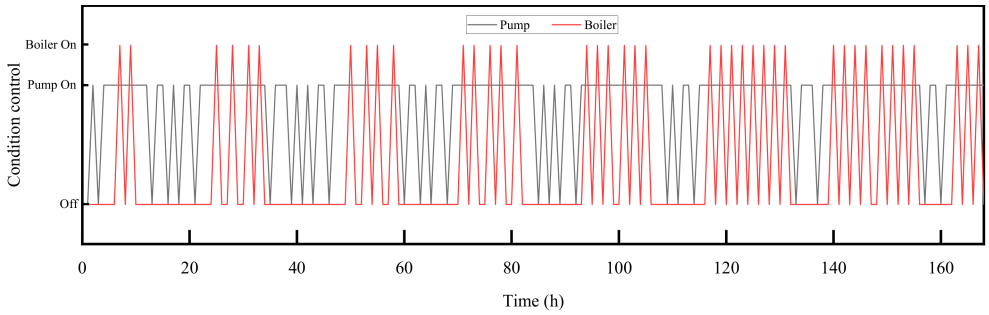

Figure 11. Control method of pumps and boilers.

- The trade-off between economic cost and comfort level

Due to the significant heterogeneity between natural gas (boiler fuel) and municipal electricity (circulating water pump) in terms of market pricing systems and carbon emission factors, the game characteristics of the system oriented by economic costs are fundamentally different from those under carbon emission optimization. As shown by the Pareto frontier in Figure 12, although the overall trend still presents nonlinear antagonism, the curvature topology of the curve and the position of the optimal decision point have shifted. The global optimal solution extracted by TOPSIS is located in a relatively high discomfort interval (approximately 150 °C·h), thereby strictly limiting the total weekly operating cost to around 60 RMB. Compared with the rigid adherence to thermal comfort under carbon emission optimization, the economic-oriented control strategy exhibits higher cost sensitivity. That is, the system tends to operate near the tolerable temperature threshold for the human body, sacrificing a slight degree of thermal comfort in exchange for higher economic benefits.

The time-series dynamic temperature response in Figure 13 verifies the above analysis. Distinctly different from the previous strategy, in which the indoor temperature was strictly controlled within a narrow range of 20.0 °C, the heat storage water tank under the economically optimal strategy operates entirely at a low energy level range of 32 °C to 48 °C. Meanwhile, the system fully utilizes the passive thermal inertia of the building itself, allowing the indoor temperature to fluctuate within a wider range from 19.2 °C to 20.4 °C. This delayed satisfaction strategy, which permits the indoor temperature to oscillate widely near the lower boundary of the comfort zone, essentially avoids the high-energy-consumption operating range of heat source equipment at the cost of partial subjective thermal perception.

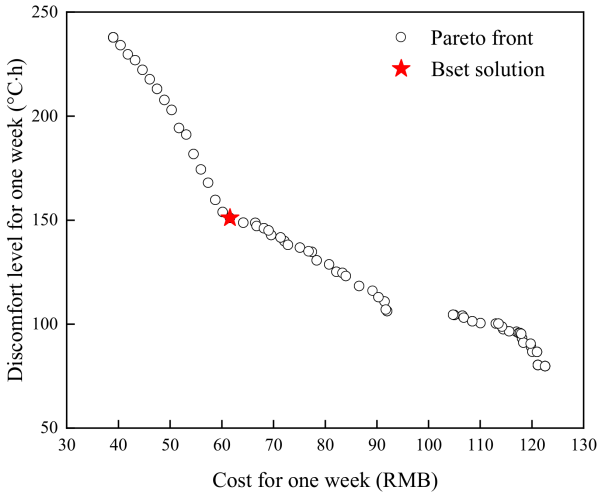

Figure 12. Pareto frontier and optimal solution of economic cost and comfort level.

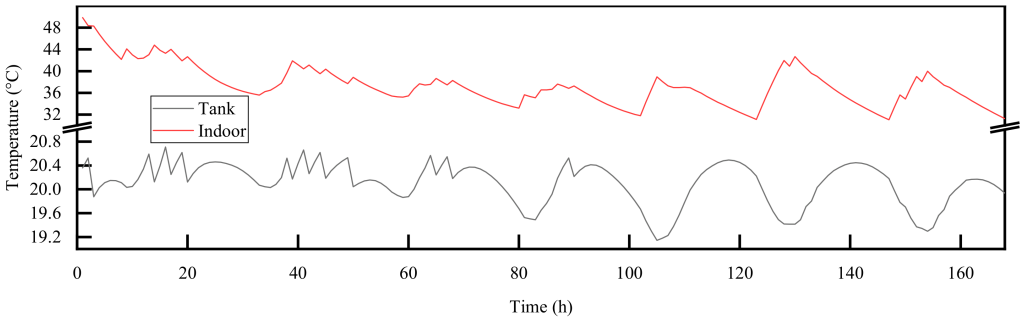

Figure 13. Temperature change.

The discrete control timing sequence of underlying equipment (Figure 14) further reveals the microscopic implementation mechanism of such economic operation. A clear comparison with the previous pulse density shows that the ignition actions of the heat source boiler (red line) become extremely sparse and brief. Instead of maintaining the water tank temperature at a full level in real time, the system keeps the circulating water pump running continuously for a long period to fully utilize the low-grade waste heat inside the water tank. The boiler is only forced to provide short-term thermal compensation when both the water tank temperature and indoor temperature drop below the absolute lower limit of the hysteresis dead zone, posing a risk of system thermal collapse. This minimalist asynchronous coordination logic of non-operation unless necessary is the key for the system to achieve substantial cost reduction under extremely cold weather conditions.

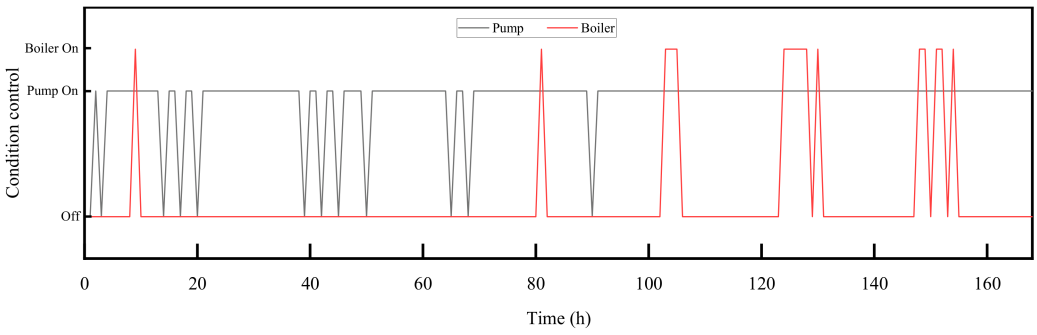

Figure 14. Control method of pumps and boilers.

4.4.2. Full-Dimensional Collaborative Optimization and TOPSIS Decision Extraction of Carbon-Economy-Comfort

Furthermore, this study conducts a full-dimensional collaborative optimization with total carbon emissions, operational economic cost, and heating discomfort degree as evaluation dimensions. As shown by the three-dimensional Pareto frontier curve in Figure 15, the optimization results exhibit a characteristic of highly collapsing toward the frontier of the dual objectives of economy and comfort in terms of spatial topological morphology. This phenomenon profoundly reveals the underlying multi-physics field coupling mechanism of the system: natural gas and municipal electricity consumption show a high linear positive correlation in environmental cost and economic cost, forming a strong synergistic force in the three-dimensional dimensionality-reduction optimization and jointly imposing an intense constraint on thermal comfort. Under these dual constraints, the three-dimensional global optimal solution extracted by the TOPSIS method presents extreme sensitivity to both cost and energy consumption. That is, the system tends to achieve a substantial reduction in operational cost by making a slight compromise on subjective thermal perception while maintaining the basic environmental threshold.

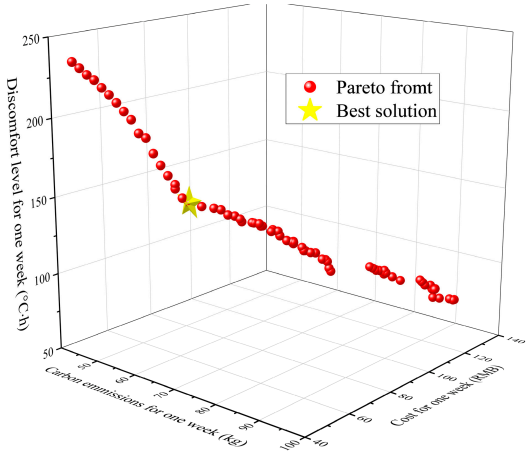

Figure 15. Full-dimensional collaborative optimization results of carbon-economy-comfort.

It is worth noting that within the boundary of the current model, both carbon emissions and economic costs are driven by boiler fuel consumption. They represent two measurement methods for the same physical quantity, and their high consistency is an objective reflection of the physical system and economic pricing mechanism, rather than an artificial construction of the optimization algorithm.

4.4.3. Comprehensive Benefit Evaluation of Full Cycle Under Extreme Variable Working Conditions

From the temperature dynamic tracking in Figure 16, it can be seen that the global optimal strategy completely abandons the redundant setting of blindly maintaining a high water tank temperature adopted in the baseline strategy. The system fully activates the passive thermal inertia of the building itself, allowing the indoor temperature to fluctuate widely along the lower edge of the comfort range of 19.5 °C to 20.5 °C. The corresponding micro operational logic indicates that the underlying equipment strictly implements asynchronous and cooperative relay control. The start-stop frequency of the heat source boiler is greatly reduced, and the system makes full use of low-grade residual heat in the water tank. Extremely infrequent short-term supplementary heating is only triggered when the indoor temperature approaches the absolute lower limit threshold, thereby fully implementing the energy-saving principle of "no ignition unless necessary".

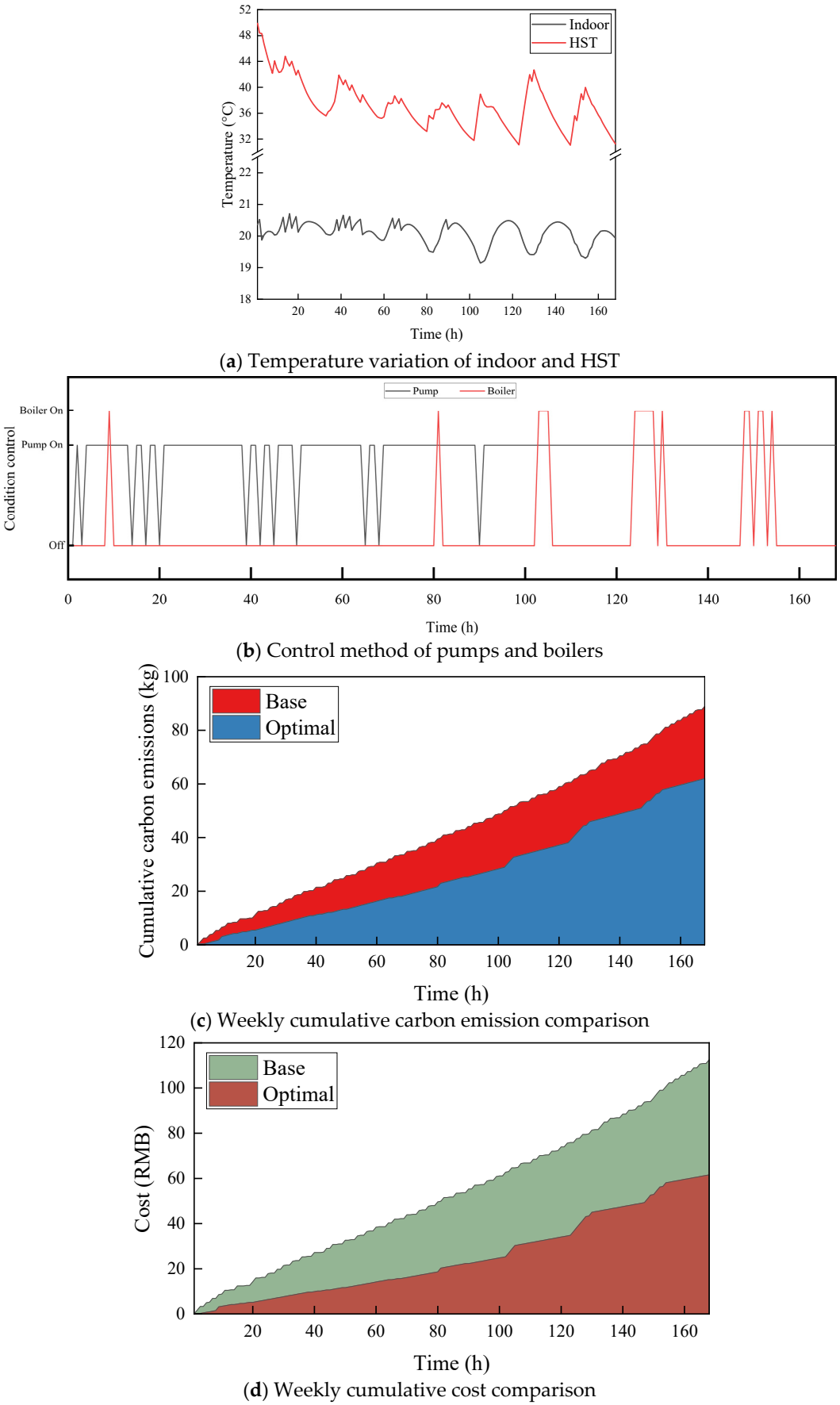

(**a**) Temperature variation of indoor and HST

(**b**) Control method of pumps and boilers

(**c**) Weekly cumulative carbon emission comparison

(**d**) Weekly cumulative cost comparison

Figure 16. Planning and comparison of system operating parameters.

The deep coupling between the above macro flexible boundary setting and micro rigid start-stop operation ultimately generates remarkable cumulative engineering benefits. The stepwise rising cumulative curves in Figure 16c,d intuitively quantify these outcomes: compared with the traditional constant-temperature baseline strategy, the three-dimensional global optimization strategy achieves a total carbon emission reduction of up to 30.3% and a total operating cost saving of 45.3% within the 168-h extreme cold disturbance cycle. This leapfrog improvement in comprehensive performance not only verifies the optimization-seeking capability of multi-objective heuristic algorithms in the regulation of complex energy digital twins, but also theoretically and practically confirms that accurately capturing and utilizing the co-evolution law of carbon-economic indicators is the most effective approach to resolve the problems of high energy consumption, high carbon emissions, and high operating costs of distributed heating systems in cold regions.

5. Conclusions

This study addresses the challenges faced by renewable heating systems in severely cold regions under extreme off-design conditions, including large thermal inertia, strong multi-variable coupling, and difficulties in dynamic coordination between supply and demand sides. Taking a distributed heating system integrating solar thermal collection and ammonia-doped natural gas combustion in parallel as the research object, a systematic study was conducted covering dynamic modeling, data-driven surrogate model construction, and multi-objective intelligent optimal control. It should be emphasized that all results presented in this study are derived from numerical simulations based on a lumped-parameter physical model and a data-driven neural network surrogate, rather than from field experiments on a physical prototype. The simulation model was validated against published reference data for individual components. The main conclusions are as follows:

(1) A multi-layer fully connected neural network surrogate model with a residual autoregressive structure was constructed. By setting the prediction target as temperature increments rather than absolute temperatures, the model preserves thermal inertia. During 168 h of continuous rolling prediction, the root mean square error for indoor temperature is 0.1603 °C and for storage tank temperature is 0.6124 °C, with no error divergence in the blind forecast period, demonstrating that the model possesses high accuracy and strong robustness in replacing high-dimensional physics-based models for real-time inference.

(2) A parameterized rule-based optimization framework was proposed, taking the slope and intercept of the climate-compensated heating curve and the temperature control dead-band as decision variables. By coupling the NSGA-II algorithm with the surrogate model, the multi-dimensional conflict relationships among carbon emissions, economic cost, and thermal comfort were deconstructed. Two-dimensional Pareto front analysis shows that under the carbon–comfort trade-off, the TOPSIS best-compromise solution achieves 80.62 kg CO_2 emissions per week while limiting discomfort to 104.85 °C·h; under the cost–comfort trade-off, the optimal strategy compresses the operating cost to approximately 60 CNY but allows indoor temperature to fluctuate broadly between 19.2 °C and 20.4 °C, revealing the deep substitution rule between cost and comfort.

(3) Three-dimensional all-objective collaborative optimization further reveals that carbon emissions and economic cost are highly linearly aligned at the physical source, jointly exerting strong suppression on comfort. The globally optimal strategy extracted by TOPSIS completely abandons the redundant constant high-temperature setpoint. By substantially reducing the boiler start–stop frequency, deeply utilizing residual heat in the water tank and the building's thermal mass, this strategy achieves a 30.3% reduction in total carbon emissions and a 45.3% saving in total operating cost compared

with the conventional constant-temperature baseline strategy over a 168 h extreme cold disturbance period, fully validating the superior efficacy of the multi-objective intelligent control strategy.

(4) The annual carbon emission assessment of the system demonstrates that ammonia co-firing technology can reduce annual carbon emissions from approximately 560 kg to 510 kg while maintaining the same heating effect, revealing the significant potential of clean fuel substitution synergized with intelligent control to demonstrate the potential of ammonia-co-firing in reducing direct CO_2 emissions.

The findings of this study are specific to the investigated system configuration, building characteristics, and climatic conditions. The methodological framework—integrating physics-informed simulation, residual autoregressive neural surrogates, and multi-objective evolutionary optimization—is broadly applicable to other cold-region heating systems with appropriate parameter adjustments. For buildings with lower thermal mass (e.g., light-frame construction), the benefit of passive thermal buffering would be reduced, and more aggressive active control may be required. For milder climates, the solar fraction would increase, and the optimal ammonia blending ratio might differ. Future work should extend this framework to (i) multi-zone buildings, (ii) other cold cities, and (iii) systems with different renewable energy integrations.

In addition, the current economic-cost model mainly considers natural gas fuel costs and does not include factors such as the power consumption of circulating water pumps and the service-life loss of equipment caused by start-stop cycles. Under the constant-flow pump control strategy, the impact of pump power consumption is relatively small. However, refined modeling of start-stop losses will be an important direction for improving the engineering practicality of the optimization framework in the future.

Author Contributions: W.L.: Investigation, Software, Visualization, Writing—original draft. X.S.: Writing—review & editing. Y.C.: Methodology, Project administration. P.L.: Supervision. C.Z.: Supervision. All authors have read and agreed to the published version of the manuscript.

Funding: The authors gratefully acknowledge the National Key R&D Program of China under the key special project (No.: 2024YFC3809304-3), the Heilongjiang Provincial Science and Technology Innovation Base Incentive Project (No. JD24B012), Heilongjiang Provincial Postdoctoral Science Foundation (No. LBH-Z25149), and CSCEC Science and Technology R&D Program (Grant No. CSCEC-2025-Z-30).

Data Availability Statement: The data presented in this study are available on request from the corresponding author due to legal reasons.

Conflicts of Interest: The authors declare no conflicts of interest.

Abbreviations

The following abbreviations are used in this manuscript:

A	area (m^2)
C	relative closeness
c_p	specific heat capacity J/(kg·K)
d	distance
f	objective factor
H	height (m)
h	Heat transfer coefficient ($W/(m^{2\cdot}K)$)
I	solar radiation intensity (W/m^2)
K	heat transfer coefficient (W/(K))
LHV	Lower heating value (MJ/kg)
M	mass (kg)
MSE	mean squared error

P	power (W)
Q	heat (W)
T	temperature (K)
t	time (s)
V	volume (m^3)
x	ammonia mixing ratio (%)
act	active
avg	average
boil	boiler
coll	collect
f	fluid
HST	hot water storage tank
hx	heat exchanger
in	indoor
out	outdoor

Appendix A

Table A1. Neural network training configuration and hyperparameters.

Parameter	Value	Parameter
Network architecture	Input layer–128–64–32–Output layer (2 neurons)	Network architecture
Activation function (hidden layers)	ReLU	Activation function (hidden layers)
Activation function (output layer)	Linear	Activation function (output layer)
Optimizer	Adam	Optimizer
Loss function	Mean squared error (MSE)	Loss function
Learning rate	0.001	Learning rate
Batch size	32	Batch size
Training epochs	200 (with early stopping)	Training epochs
Early stopping patience	20 epochs (no improvement on validation loss)	Early stopping patience
Training set	Hours 1–120	Training set
Validation set	Hours 97–120 (last 24 h of training period)	Validation set
Blind test set	Hours 121–168 (48-h blind forecast)	Blind test set
Data normalization	Z-score standardization, fitted on training set only	Data normalization
Random seed	42 (for weight initialization only; no random shuffling)	Random seed
Number of repeated training runs	5 (averaged results reported)	Number of repeated training runs

Table A2. Test Room Parameters.

Parameter	Value	Unit	Introduction
Room area (A_{room})	20	m^2	Heated room building area
Room height (H_{room})	2.8	m	Room height
Air density (ρ_{air})	1.2	kg/m^3	Indoor air density under standard conditions
Specific heat capacity of air ($c_{p,air}$)	1005	J/(kg·K)	Specific heat capacity of indoor air
Average heat transfer coefficient of envelope structure (h_{env})	0.3	W/(m^2·K)	High thermal insulation standard for Harbin passive houses

Table A3. Hot water storage tank.

Parameter	Value	Unit	Introduction
Volume of HST (V_{HST})	1000	L	Total volume of HST
Water density (ρ_{water})	1000	kg/m^3	Standard density of liquid water
Specific heat capacity of air ($c_{p,water}$)	4180	J/(kg·K)	Heat transfer coefficient of HST Insulation Layer
Heat transfer coefficient of HST insulation layer ($h_{HST,ins}$)	0.5	W/(m^2·K)	Heat transfer coefficient of high-efficiency thermal insulation materials
Water tank surface area (A_{HST})	4	m^2	Estimated external surface area of the water storage tank

Table A4. Collector parameters.

Parameter	Value	Unit	Introduction
Collector area	6	m^2	Total daylight collection area of flat-plate solar collector
Zero-loss efficiency	0.75	-	The theoretical maximum efficiency of the collector without temperature difference loss
First-order loss coefficient	3.5	$W/(m^2 \cdot K)$	Linear coefficient of heat loss of collector varying with temperature difference

Table A5. Boiler parameters.

Parameter	Value	Unit	Introduction
Boiler nominal input power (P_{comb})	4000	W	Rated input power of natural gas-ammonia blended boiler
Ammonia mixing ratio (x)	20	%	Volume mixing parameter
Ammonia-doped combustion efficiency	0.85	-	Simplified comprehensive thermal efficiency of boiler (Considering combustion characteristics after ammonia blending)

Table A6. Radiator parameters.

Parameter	Value	Unit	Introduction
Overall Heat Transfer Coefficient of Radiator	50	W/K	Indoor comprehensive heat transfer coefficient

Table A7. Heating control strategy.

Parameter	Value	Unit	Introduction
Room target temperature ($T_{in,target}$)	21	°C	Indoor heating design temperature
Room temperature control hysteresis range	0.5	°C	Temperature dead band (20.5~21.5 °C) for preventing frequent start-stop of the load pump
HST target temperature	50	°C	Set value of holding temperature for hot water storage tank
HST temperature control hysteresis range	3	°C	Temperature dead zone (47~53 °C) to prevent frequent start-stop of the boiler

Table A8. NSGA-II parameter settings.

Parameter	Value
Population size	50
Maximum generations	200
Crossover operator	Simulated Binary Crossover (SBX)
Crossover probability	0.9
Crossover distribution index	15
Mutation operator	Polynomial Mutation (PM)
Mutation probability	0.1
Mutation distribution index	20
Selection mechanism	Tournament selection (tournament size = 2)
Elitism	Elite count = 2 (top individuals preserved)
Constraint handling	Feasible solution preservation strategy
Number of independent runs	5

Table A9. Decision variable bounds.

Decision Variable	Lower Bound	Upper Bound	Unit
Water tank set temperature ($T_{tank,set}$)	35	60	°C
Room temperature hysteresis dead-band ($\Delta T_{hysteresis}$)	0.3	1.5	°C
Climate compensation curve slope	0.2	0.9	—
Climate compensation curve intercept	10	30	°C

References

1. Wang, X.; Jia, Y.; Zuo, D. Study on Optimization of Two-Stage Phase Change Heat Storage Coupled Solar-Air Source Heat Pump Heating System in Severe Cold Region. *Energy Eng*. **2025**, *122*, 1603–1627. [CrossRef]
2. Shi, L.; Liu, Y.; Sun, C.; Guo, Y.; Wang, D.; Liu, Y.; Si, P.; Jiang, Q.; Duan, Q.; Wang, C. Energy Solution for Rural Household in Remote Cold Regions: An Innovative Photovoltaic-Based Thermal Energy Storage System. *Energy Convers. Manag*. **2025**, *343*, 120216. [CrossRef]
3. Qu, L.; Wang, D.; Zhou, Y.; Yuan, W.; Liu, Y.; Fan, J. A New Capacity Design Method for PV-ASHP System Based on Energy Flow Mechanism and Energy Supply-Demand Balance. *Renew. Energy* **2025**, *239*, 121995. [CrossRef]
4. Dai, B.; Li, X.; Liu, X.; Han, J.; Zhang, T.; Zou, T.; Liu, S. Multi-Stage Liquid Separation Condensation High-Temperature Heat Pump System Using Zeotropic Working Fluid: System Construction and Comparison with Traditional Solutions. *Energy* **2025**, *330*, 136850. [CrossRef]
5. Dai, B.; Wang, X.; Liu, S.; Wang, M.; Xie, S.; Zhang, T.; Li, C. Ejector Subcooling Carbon Dioxide Combined Heating and Cooling System Driven by Waste Heat: Energy, Exergy, Environment and Economic Evaluation. *Energy Convers. Manag*. **2025**, *333*, 119782. [CrossRef]
6. Chen, S.; Chang, T.; Yang, Y. Summer Thermal and Energy Performances Assessment of a Modular Hydronic Thermal Barrier Wall for Ultra-Low Energy Buildings—A Field Experimental Study. *Appl. Therm. Eng*. **2024**, *236*, 121491. [CrossRef]
7. Yang, X.; Zou, T.; Xu, Y.; Chen, F.; Luo, H.; Ullah, S.; Li, R. Research Dynamics and Applications of Tracking Technology and Devices in Solar Energy Utilization System. *Sustain. Energy Technol. Assess*. **2025**, *75*, 104256. [CrossRef]
8. Zhang, Z.; Cao, Y.; Qin, S.; Wang, Z.; Gao, W.; Jia, G.; Jin, L. Optimization of Design Parameters and Operation Conditions of Solar-Air Source Heat Pump Coupled System for Rural Buildings in Cold and Severe Cold Regions. *Sol. Energy* **2025**, *286*, 113147. [CrossRef]
9. Liang, X.; Yang, J.; Zhu, J.; Peng, M. Understanding and Coping with Uncertainties in District Heating Systems: A Multi-Pathway Review from Probabilistic Modeling to Intelligent Integration. *Energy Build*. **2025**, *349*, 116514. [CrossRef]
10. Liu, C.; Wang, H.; Wang, Z.; Liu, Z.; Tang, Y.; Yang, S. Research on Life Cycle Low Carbon Optimization Method of Multi-Energy Complementary Distributed Energy System: A Review. *J. Clean. Prod*. **2022**, *336*, 130380. [CrossRef]
11. Liu, Z.; Fan, G.; Sun, D.; Wu, D.; Guo, J.; Zhang, S.; Yang, X.; Lin, X.; Ai, L. A Novel Distributed Energy System Combining Hybrid Energy Storage and a Multi-Objective Optimization Method for Nearly Zero-Energy Communities and Buildings. *Energy* **2022**, *239*, 122577. [CrossRef]
12. Zhao, J.; Cai, S.; Luo, X.; Tu, Z. Dynamic Characteristics and Economic Analysis of PEMFC-Based CCHP Systems with Different Dehumidification Solutions. *Int. J. Hydrogen Energy* **2022**, *47*, 11644–11657. [CrossRef]
13. Kaabinejadian, A.; Pozarlik, A.; Acar, C. A Systematic Review of Predictive, Optimization, and Smart Control Strategies for Hydrogen-Based Building Heating Systems. *Appl. Energy* **2025**, *379*, 124994. [CrossRef]
14. Kong, X.; Du, X.; Xu, Z.; Xue, G. Predicting Solar Radiation for Space Heating with Thermal Storage System Based on Temporal Convolutional Network-Attention Model. *Appl. Therm. Eng*. **2023**, *219*, 119574. [CrossRef]
15. Khayrullaev, H.; Omle, I.; Kovács, E. Prediction of Heat Transfer in Building Walls of Different Materials Using Neural Networks and Finite Difference Methods. *Eng* **2026**, *7*, 173. [CrossRef]
16. Frison, L.; Kollmar, M.; Oliva, A.; Bürger, A.; Diehl, M. Model Predictive Control of Bidirectional Heat Transfer in Prosumer-Based Solar District Heating Networks. *Appl. Energy* **2024**, *358*, 122617. [CrossRef]
17. Hong, F.; Zhao, Y.; Ji, W.; Hao, J.; Fang, F.; Liu, J. A Dynamic Migration Route Planning Optimization Strategy Based on Real-Time Energy State Observation Considering Flexibility and Energy Efficiency of Thermal Power Unit. *Appl. Energy* **2025**, *377*, 124575. [CrossRef]
18. Bai, Y.; Li, C.; Prasad Jenne, S.; Zhang, S.; Wang, J. Thermal Comfort Driven Space Heating Control via Hierarchical State Machine Strategy Interacting with Multiphysics Simulation. *Energy Build*. **2024**, *323*, 114806. [CrossRef]
19. Liu, L.; Wang, C.; Tu, R. Study of a Multi-Objective Optimization Model for Load Distribution Strategy in A Centralized Heating System with Multi-Heat Source. *Appl. Therm. Eng*. **2025**, *266*, 125675. [CrossRef]
20. Wang, Z.; Li, L.; You, Y.; Yan, R.; Gu, Y. High and Low Pressure Cylinder Bypass Heat Supply Unit Operation Characteristics with Coordinated Intermediate Pressure Valve Control. *Case Stud. Therm. Eng*. **2025**, *75*, 107131. [CrossRef]
21. Liu, Z.; Chen, Y.; Cheng, K.; Fei, T.; Qin, J.; Mei, H. Assessment of Lunar Base Energy System with Lunar Limited Resources as Variable-Composition Mixed Working Fluids: Working Fluid Selection, Component Variation Law, and Full-Cycle Operational Characteristics. *Energy Convers. Manag*. **2026**, *351*, 121018. [CrossRef]
22. Liu, Z.; Wu, M.; Zhang, X.; Sun, Z.; Wang, Y.; Liu, P.; Fei, T.; Qin, J.; Mei, H. Research on a Lunar Base Combined Thermodynamic Cycle System Integrating Stirling Engines: Cold Energy Migration, Day-Night Thermodynamic Performance, and Power to Weight Ratio. *Energy* **2026**, *361*, 142069. [CrossRef]

23. Liu, Z.; Chen, Y.; Li, J.; Liu, W.; Fei, T.; Qin, J.; Mei, H. Assessment of Energy Generation Mechanism and Daytime-Nighttime Operation Characteristics of Lunar Base Solar-Hydrogen Complementary Energy System. *Energy* **2026**, *356*, 141203. [CrossRef]
24. Qiao, S.; Fu, J.; Liu, B.; Liu, Z.; Zhang, N.; Qin, J. Multi-Objective Optimization Scheduling of off-Grid Combined Heat, Power, and Hydrogen Production Systems in Cold Regions under Fluctuating Demand: The Case of Korla. *Energy* **2025**, *338*, 138956. [CrossRef]
25. Araújo, A.; Pereira, V. Solar Thermal Modeling for Rapid Estimation of Auxiliary Energy Requirements in Domestic Hot Water Production: On-off Flow Rate Control. *Energy* **2017**, *119*, 637–651. [CrossRef]
26. Hou, Y.; Chang, H.; Xia, Y.; Liu, H.; Zhang, Y.; Wang, N.; Lv, B. Simulation-Based Performance and Limitations of Photovoltaic and Solar Water Heating Systems in a Passive-Designed Rural House. *Buildings* **2026**, *16*, 3173. [CrossRef]
27. Liu, B.; Zhu, H.; Wang, Z.; Liu, Z.; Liu, Z.; Qiao, S.; Wang, C.; Cheng, K.; Qin, J. Customizing Thermal Regulation of Composite Phase Change Materials Using Triply Periodic Minimal Surfaces: A Coupled Simulation and Intelligent Algorithms Optimization Framework. *Energy Convers. Manag.* **2026**, *354*, 121200. [CrossRef]
28. Peng, Y.; Lin, X.; Liu, J.; Su, W.; Zhou, N. Machine Learning Prediction of ORC Performance Based on Properties of Working Fluid. *Appl. Therm. Eng.* **2021**, *195*, 117184. [CrossRef]
29. Tharushi Imalka, S.; Yang, R.J.; Zhao, Y. Machine Learning Driven Building Integrated Photovoltaic (BIPV) Envelope Design Optimization. *Energy Build.* **2024**, *324*, 114882. [CrossRef]
30. Dong, B.; Wang, S.; Thorin, E.; Sun, Q.; Li, H. Negative Emission Potential from Biomass/Waste Combined Heat and Power Plants Integrated with CO2 Capture: An Approach from the National Perspective. *J. Clean. Prod.* **2024**, *467*, 142917. [CrossRef]
31. Liu, Z.; Wang, Z.; Cheng, K.; Wang, C.; Ha, C.; Fei, T.; Qin, J. Performance Assessment of Closed Brayton Cycle-Organic Rankine Cycle Lunar Base Energy System: Thermodynamic Analysis, Multi-Objective Optimization. *Energy* **2023**, *278*, 127936. [CrossRef]
32. Wang, Z.; Liu, Z.; Zheng, K.; Cheng, K.; Wang, C.; Wang, Z.; Qin, J. Evaluation of Phase Change Material-Based Heat Storage Liquid Cold Plate for Thermal Pulse Resistance: Topology Optimization, Performance Comparison, and Characteristics Research. *Therm. Sci. Eng. Prog.* **2025**, *64*, 103785. [CrossRef]
33. Liu, Z.; Wang, J.; Wang, Z.; Yan, T.; Cheng, K.; Xu, J.; Qin, J. Numerical Analysis on Lunar Heat Storage System: Multi-Objective Optimization, Heat Storage Capacity, and Thermal Insulation Performance. *J. Energy Storage* **2023**, *59*, 106508. [CrossRef]
34. Li, K.; Liu, Z.; Xu, J.; Liu, H.; Xu, S.; Wang, C.; Qin, J. Evaluation of High-Speed Aircraft Thermal Management System Based on Spray Cooling Technology: Energy Analysis, Global Cooling, and Multi-Objective Optimization. *Appl. Therm. Eng.* **2023**, *229*, 120632. [CrossRef]
35. Shi, C.; Wang, M.; Yang, J.; Liu, W.; Liu, Z. Performance Analysis and Multi-Objective Optimization for Tubes Partially Filled with Gradient Porous Media. *Appl. Therm. Eng.* **2021**, *188*, 116530. [CrossRef]
36. Adun, H.; Adedeji, M.; Adebayo, V.; Shefik, A.; Bamisile, O.; Kavaz, D.; Dagbasi, M. Multi-Objective Optimization and Energy/Exergy Analysis of a Ternary Nanofluid Based Parabolic Trough Solar Collector Integrated with Kalina Cycle. *Sol. Energy Mater. Sol. Cells* **2021**, *231*, 111322. [CrossRef]
37. Guo, F.; Qin, J.; Ji, Z.; Liu, H.; Cheng, K.; Zhang, S. Performance Analysis of a Turbofan Engine Integrated with Solid Oxide Fuel Cells Based on Al-H2O Hydrogen Production for More Electric Long-Endurance UAVs. *Energy Convers. Manag.* **2021**, *235*, 113999. [CrossRef]

Disclaimer/Publisher's Note: The statements, opinions and data contained in all publications are solely those of the individual author(s) and contributor(s) and not of MDPI and/or the editor(s). MDPI and/or the editor(s) disclaim responsibility for any injury to people or property resulting from any ideas, methods, instructions or products referred to in the content.